



## Enhanced Diffusivity in Metal-Organic Frameworks for Use as a Drug Delivery System

A Major Qualifying Project  
Submitted to the Faculty of  
Worcester Polytechnic Institute  
In partial fulfilment of the requirements  
For the degree of Bachelor of Science  
In  
Chemical Engineering

By  
Matt Bennett  
John Palumbo  
Corey Scott  
Colby Whitcomb

Date: March 2nd, 2018

Project Advisor: Andrew Teixeira

*This report represents the work of WPI undergraduate students submitted to the faculty as evidence of a degree requirement. WPI routinely publishes these reports on its website without editorial or peer review. For more information about the projects program at WPI, see <http://www.wpi.edu/Academics/Projects>.*

## Abstract

The pharmaceutical industry is undergoing a transformative shift toward personalized medicine and new methods for controlled delivery of those drugs are necessary. MOFs are an exciting potential sorbent due to their extremely high surface areas (1,000 m<sup>2</sup>/g and 10,000 m<sup>2</sup>/g) and ultrafine molecular sieving ability. In this project, we designed, constructed, and validated a system and mathematical model for assessing the drug release profiles from porous media. The work culminates with a systematic perspective identifying the need for stable, size-tunable frameworks that could serve as an excellent and effective drug delivery system.

## Acknowledgements

We would like to thank the Chemical Engineering Department at WPI. The Teixeira Lab, namely Jim Vicens, was instrumental to us learning the techniques and lab methods for completing this project. Finally, we would like to thank Professor Andrew Teixeira for his continued help and guidance. Without him, we would not have been able to complete this project.

## Executive Summary

Metal-Organic Frameworks (MOFs) are a high surface area, microporous class of crystals, which are made up of metal atoms connected by organic chain linkers as can be seen in Figure 1. The study of MOFs was derived from the study of zeolites, another high surface area material, widely used for catalysis. Recently, MOFs have been studied at length for many applications including batteries, substance detection, gas storage, drug delivery, and many more.

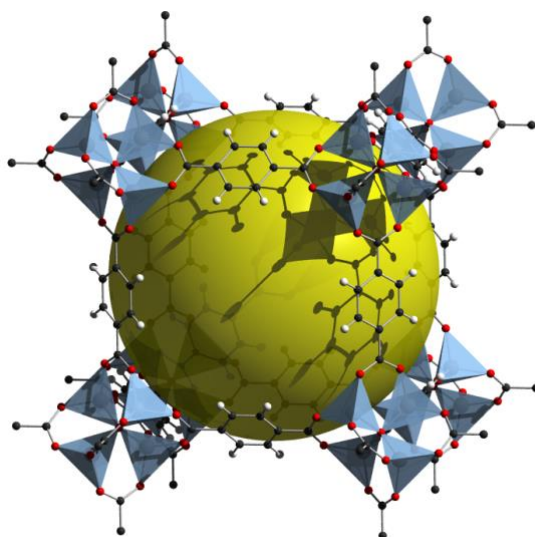


Figure 1: Metal-Organic Framework Schematic (Red: metal atoms, Black and White: organic linker atoms, Yellow: internal volume) (Boehle)<sup>1</sup>

This project attempts to use the internal cage of the MOF to store an active pharmaceutical ingredient (API), and investigate the diffusive properties out of the MOF and MOF-like materials (zeolites) for use as a drug delivery system. To achieve this goal, an HPLC system was modified to achieve an alternate flow through a zero-length continuously stirred tank reactor (CSTR) with minimal dead volume. The sorbate used in this project is the common pharmaceutical acetaminophen (also known as Tylenol, or paracetamol). The absorbance of the sorbate was measured continuously and recorded to be later analyzed with a numerical approach through a Matlab model.

The Matlab model was designed to fit a partial differential equation derived by Brandani & Ruthven (1995).<sup>22</sup> This model had a few parameters which could be modified to fit the data. These parameters were  $L$ , dead volume, diffusivity constant, pore size, and flow rate.  $L$  is a fitting variable that condenses a few other variables in the equation derived by Brandani and Ruthven and is the ratio of the cell washout time to the diffusion time.<sup>22</sup> The model was incentivized to minimize the difference between the raw data collected from the HPLC and the generated model with a final outcome being the intraparticle diffusion coefficient.

As a system validation, common zeolites were also tested (Zeolite HY, and an ion exchanged Zeolite-NaY) with the sorbate to obtain desorption profiles to compare to. The results from an example run can be seen below in Figure 2. The yellow line shows the model generated by the Matlab script, and the blue line shows the raw data from the HPLC. It should be noted that beyond 20 minutes, the concentration is so low that it can easily be affected by noise in the detector. Therefore, the model was fit by weighting the first 20 minutes more heavily. From this model, it could be estimated that the diffusivity constant of  $1.4 * 10^{-13} \frac{m^2}{s}$ , and an  $L$  “fitting factor” of 4500.

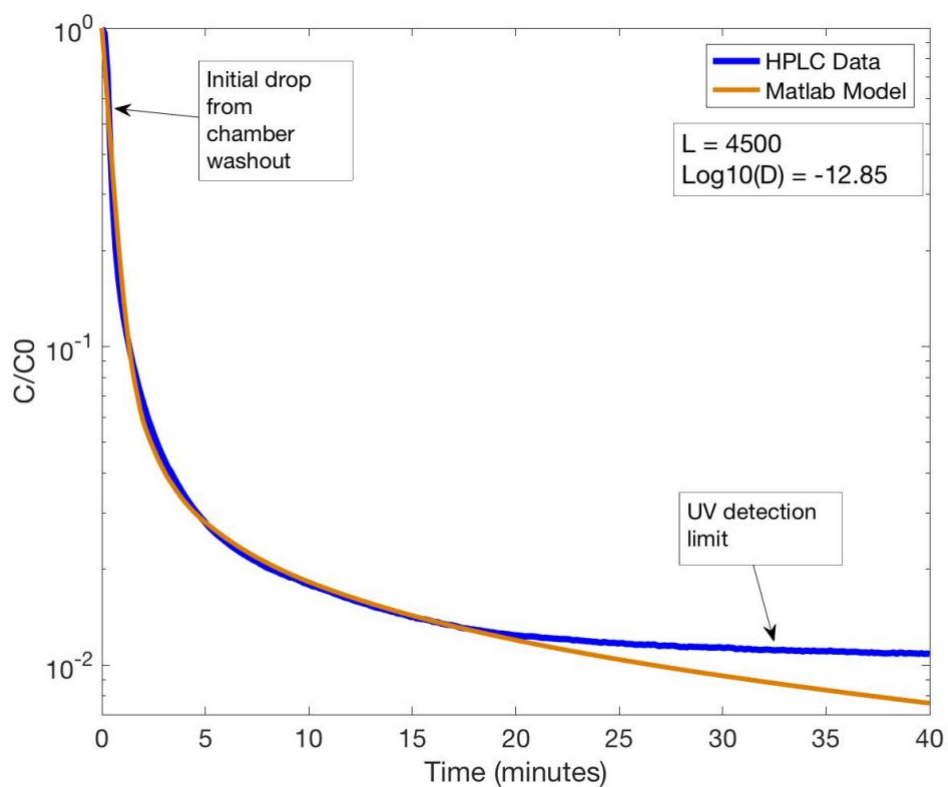


Figure 2: Semi-Log Plot of normalized concentration versus time over-layed with Matlab Model of ion exchanged Zeolite-NaY

Due to the nature of the MOF examined in this project, it was not possible to achieve a smooth desorption profile. This paper demonstrates the preliminary data and results about the use of MOFs for drug delivery systems.

## Table of Contents

Abstract.....	1
Acknowledgements.....	2
Executive Summary.....	3
Table of Contents.....	6
List of Tables.....	8
List of Figures.....	9
1.0 Introduction.....	11
2.0 Literature Review.....	13
2.1 Diffusivity.....	13
2.2 Residence Time Model.....	16
2.3 High Performance Liquid Chromatography (HPLC) System and Uses.....	19
2.4 Zero-Length Column Modeling.....	22
2.5 Mathematical Model.....	26
2.6 Zeolites.....	28
2.7 Metal Organic Frameworks (MOFs).....	29
2.7.1 Characteristics.....	29
2.7.2 History of MOFs.....	31
2.7.3 MOF Synthesis.....	34
2.7.4 IRMOFs.....	35
2.7.5 MOF Imaging.....	35
2.8 MOF Applications.....	37
2.8.1 Drug Delivery.....	37
2.8.2 Pesticide Detection and Concentration.....	42
2.8.3 Anti-Corrosion Coatings.....	42
2.8.4 Bifunctional Oxygen Electrocatalysts for Metal Air Batteries.....	43
2.8.5 Natural Gas Storage.....	43
3.0 Experimental.....	45
3.1 HPLC Configuration Optimization.....	45
3.2 ZLC System Validation.....	47
3.3 Paracetamol Extraction.....	48
3.3.1 Paracetamol Characterization.....	48
3.4 Zeolite Ion Exchange.....	50

3.5 Zeolite Diffusion Trials.....	51
3.6 MOF Synthesis.....	52
3.6.1 MOF Characterization .....	53
3.7 MOF Trials.....	54
3.8 Mathematical Model .....	55
3.8.1 System Optimization.....	55
3.8.2 Diffusivity Modeling .....	59
3.9 Safety .....	61
4.0 Results and Discussion .....	62
4.1 Particle Size and Volume Distribution .....	62
4.2 Analysis of Methods Used for Modelling.....	64
4.3 Diffusion Measurements in Zeolite System Validation.....	65
4.3.1 Approximate Analytical Model Fitting.....	65
4.3.2 Numerical Solution Fits of Zeolite Runs .....	67
4.4 IRMOF Results .....	69
4.4.1 IRMOF Diffusion Coefficient Model .....	69
4.5 Impurities in MOF .....	73
5.0 Conclusion .....	76
5.1 Main Findings .....	76
5.2 Future Work .....	76
6.0 References.....	77
Appendix A: Raw Data.....	81
Appendix B: Matlab Code .....	89
Script 1: Residence times and dead volume for system validation.....	89
Script 2: Numerical_PDE_MAIN.m.....	97
Script 3: bvpscripts.m .....	99
Script 4: ZLC_Fits.m .....	101
Appendix C: SDS Sheets .....	102

## List of Tables

Table 1: Comparison of diffusivities; gas-in-gas, liquid-in-liquid, and solid-in-solid .....	14
Table 2: Uptake time comparison based on Diffusion Coefficient of Zeolite-Y .....	67
Table 3: Diffusion coefficient comparison between Zeolite-Y and Zeolite-NaY .....	67
Table 4: Uptake time comparison based on Diffusion Coefficient of Zeolite-Y .....	69
Table 5: Diffusion coefficient comparison between Zeolite-Y and Zeolite-NaY .....	69
Table 6: IRMOF-1 and Blank Diffusion Coefficient Values.....	71
Table 7: Comparing Wilke-Chang Relationship to Experimental Data .....	72

## List of Figures

Figure 1: Metal-Organic Framework Schematic (Red: metal atoms, Black and White: organic linker atoms, Yellow: internal volume) (Boehle) .....	3
Figure 2: Semi-Log Plot of normalized concentration versus time over-layed with Matlab Model of ion exchanged Zeolite-NaY .....	5
Figure 3: Concentrations using impulse input into PFR (a) and CSTR (b) <sup>8</sup> .....	17
Figure 4: The Methods of Pulse and Step Injections and their Responses <sup>8</sup> .....	18
Figure 5: HPLC Setup .....	20
Figure 6: HPLC schematic showing how a solvent reservoir gets pumped through a high pressure pump to sweep the sample injection through an HPLC tube to the UV detector. ....	21
Figure 7: Diode Array Detector Schematic. Light from the lamps travel through a slit to be diffracted into a slit that can be moved depending on the wavelength needed. This beam is then split for a reference and allowed to go through the flow cell to another detector that shows the resulting intensity. ....	22
Figure 8: Basic ZLC Apparatus showing all general parts and basic flow pattern. ....	23
Figure 9: Image A shows the ZLC Column used in this project with 1/16th inch tubing going to a 1/8 <sup>th</sup> expander which is fit to the chamber at the two frits. This is then reduced on the other side downstream. Image B shows the ZLC model and all parts were purchased from Vici Valco. ....	24
Figure 10: Full uptake, saturation, and desorption profiles .....	25
Figure 11: Different Cage Geometries of Various Zeolites. These different cage shapes result in different overall network structure with different pore sizes .....	29
Figure 12: Basic MOF Structure (Red – metal atoms, Black – organic linker, Yellow – internal volume) .....	30
Figure 13: Older coordination compound (a) vs MOF structure with SBUs (b) <sup>32</sup> .....	33
Figure 14: 5-Fu Release Profile for a Zn-Based MOF <sup>38</sup> .....	38
Figure 15: RAPTA-C Release Profiles for Four ZnBDP MOFs <sup>39</sup> .....	39
Figure 16: Various HPLC configurations including the indicated components used in each trial	46
Figure 17: Paracetamol XRD Results .....	49
Figure 18: XRD results of paracetamol (white) overlayed with MDI Jade database peaks of paracetamol (green) .....	49
Figure 19: Literature UV data <sup>43</sup> .....	50
Figure 20: XRD graph of Zeolite NaY (white line) and green markers denoting the location of peaks for a Zeolite NaY from MDI Jade. ....	51
Figure 21: First IRMOF-1 Synthesis .....	53
Figure 22: Second IRMOF-1 Synthesis .....	54
Figure 23: Example of steps from HPLC. This trial is paracetamol at 198nm through IRMOF-1. ....	55
Figure 24: HPLC raw data with red box indicating desorption profile .....	55
Figure 25: Normalized Concentration on Log-Scale vs. Time .....	56
Figure 26: Residence Time (tau) vs. Inverse Flowrate showing a linear relationship in accordance with equation (20) .....	57
Figure 27: Comparison of Dead Volume for Different Configurations .....	58
Figure 28: Montage of Steps for Particle Analysis Method .....	62
Figure 29: Optical Image of MOF-5 Particles .....	62
Figure 30: Particle Diameter Distribution Using Data from ImageJ .....	63

Figure 31: Particle Volume Distribution Using Data from ImageJ .....	63
Figure 32: (A) Normalized desorption profile through an empty ZLC chamber. F = 0.5 ml/min (B) Baseline of ZLC run in Excel (blue) and fit (red), F = 0.5 ml/min .....	64
Figure 33: (A) Zeolite-Y Trial 1, F = 0.5 ml/min, (B) Zeolite-Y Trial 2, F = 0.5 ml/min .....	65
Figure 34: Normalized Raw Data for One Hour Uptake (red), Five Minute Uptake (light green), and One Minute Uptake (blue) .....	66
Figure 35: Comparison of Zeolite-NaY Uptake Times; Five Minute (light green), Five Minute Fit Line (purple), One Hour (red), One Hour Fit Line (light blue), One Minute (dark blue), and One Minute Fit Line (yellow) .....	66
Figure 36: (A) Zeolite Y trial 1, F = 0.5 ml/min, strong agreement is observed at both short and long times, (B) Zeolite NaY trial 1, F = 0.5 ml/min, (C) Zeolite NaY One Minute Uptake, F = 0.5 ml/min, (D) Zeolite NaY One Hour Uptake, F = 0.5 ml/min, note time scales .....	68
Figure 37: (A) Data Fit with IRMOF-1; dimensionless concentration (blue) and fit curve (red), F = 0.5 ml/min, (B) Data Fit with IRMOF-1; dimensionless concentration (blue) and fit curve (red), F = 0.5 ml/min, (C) Data Fit with IRMOF-1; dimensionless concentration (blue) and fit curve (red), F = 0.5 ml/min, (D) Matlab Model for MOF Diffusivity showing the short-time desorption profile model. Long time diffusion is indistinguishable from background detector noise, F = 0.5 ml/min.....	70
Figure 38: Comparison of Blank (light blue), IRMOF-1 Trial 1 (yellow), IRMOF-1 Trial 2 (gray), IRMOF-1 Trial 3 (orange), Zeolite-NaY (blue), and Zeolite-Y (light green) .....	71
Figure 39: XRD results from first (top) and second (bottom) MOF syntheses .....	73
Figure 40: XRD Pattern of Zinc Nitrate Hexahydrate .....	74
Figure 41: XRD Pattern of Terephthalic Acid .....	74
Figure 42: XRD of MOF-5 at multiple time steps in the presence of a 61% humidity environment <sup>51</sup> .....	75

## 1.0 Introduction

The next generation of pharmaceuticals will take advantage of personalized, protein-based medicine. These need to be delivered in creative, controlled ways in order to be viable in the pharmaceutical world. Metal organic frameworks (MOFs) are tunable and can potentially offer a controlled delivery method.

Recently, MOFs have been studied for their use in a variety of different settings. MOFs are a relatively new crystalline material that have similar properties to their predecessors, zeolites. MOFs consist of larger metal ions, interconnected with organic linkers. These combinations of metal ions and organic linkers create a crystalline network that allows for a very porous material. Both the metal ions and the organic linkers can be changed to create a MOF with different properties, making MOFs highly tunable. The length of the organic linker will adjust the size of the pores within the MOF. Functional groups on these linkers can also adjust the reactivity and functionality of the crystals. Finally, different metal ions will have different bonding orders, changing the overall shape of a “unit cell” (smallest single repeating unit) of the framework.

With a high surface area and extremely tunable properties, MOFs have gathered a lot of attention for their possible use in many areas of research. Drug delivery, gaseous carbon capture and storage, pesticide detection, anti-corrosion coatings, electrocatalysts for batteries are only just a few of the possible applications for MOFs in current research.<sup>2</sup>

This paper studies the diffusivity properties of one particular MOF, known as IRMOF-1 (also known as MOF-5), using a common over-the-counter pharmaceutical (Acetaminophen, also known as paracetamol). A diagram of IRMOF-1 can be seen in Figure 1.

Nanocarriers of any kind for use in drug delivery need to meet a few requirements to be efficient and worthwhile. These nanocarriers must (1) efficiently encapsulate the drugs with high

payloads, (2) control the drug's release without over or under delivery, (3) control the matrix degradation, (4) offer the capability of engineering the surface of the carrier, and (5) be detectable by conventional imaging techniques.

Some current materials being used for drug delivery include liposomes, nanoemulsions, nanoparticles or micelles. All of these materials work to some degree, but they are unsatisfactory in some regards. Therefore, better routes to drug delivery are necessary to overcome their limitations. With their extremely tunable properties, MOFs seem to be a good candidate for an improved drug delivery route.<sup>3</sup>

In this paper, to study one aspect of the drug delivery capability of IRMOF-1, the diffusive properties of paracetamol through the pores of the MOF was studied, analyzed, and modeled.

## 2.0 Literature Review

### 2.1 Diffusivity

Diffusion occurs in all gas, liquid, and solid mixtures. This molecular motion occurs due to concentration gradients in a system that push the system to move toward equilibrium. Diffusion rates are typically described by a molar or mass flux which is the amount of a particular species through a cross sectional area that is normal to the vector it is traveling along. The flux of a species is described by its concentration gradient and diffusion coefficient that is with respect to the species that it is diffusing through and the concentration gradient. This relationship is known as Fickian diffusion, which is represented by the equation:

$$J_{A,z} = -D_{AB} \frac{dC_A}{dz} \quad (1)$$

This form of the equation applies to a homogeneous system. The diffusion coefficient is a function of the pressure, temperature and composition of the system. Typically, diffusion coefficients are highest for gases and lowest for solids.

While diffusion in gas systems can be simplified fairly well due to the lack of interaction between molecules, liquid mass diffusion is a more complex system. In a liquid, molecules are tightly packed together meaning that concentration gradients can result in changes in viscosities which leads to a change in the ideality of the system (i.e. molecular interactions cannot be neglected). Two theories have been proposed to deal with these complexities. The Eyring “hole” theory assumes that the solvent atoms form a quasi-crystalline shell around a diffusing molecule with periodic holes in the lattice where solute atoms jump from vacancy to vacancy. The hydrodynamical theory states that the liquid diffusion coefficient is related to the solute mobility through the solvent. The solute’s molecular mobility is represented by the net velocity of the

molecules under the influence of a driving force. The result of combining both theories results in an equation where the diffusion coefficient is dependent on temperature and the viscosity of the solvent. Several correlations have been developed to describe certain isolated cases. An example of this is the Wilke-Chang relationship. This correlation applies to nonelectrolytes in an infinitely dilute solution and defines the diffusion coefficient as a function of the temperature, viscosity of the solvent, “association” parameter and molar mass of the solvent, and the molal volume of the solute at normal boiling point.

As mentioned before, even though liquid mass diffusion can be extremely slow, diffusion into and through a solid is much slower. This effect is shown by the table of known values of diffusion through various mediums shown below:

Table 1: Comparison of diffusivities; gas-in-gas, liquid-in-liquid, and solid-in-solid<sup>4</sup>

<b>Phase</b>	<b>Diffusivity Coefficient Range</b>
Gases	$5.6 * 10^{-6}$ to $10^{-5} \frac{m^2}{s}$
Liquids	$10^{-10}$ to $10^{-9} \frac{m^2}{s}$
Solids	$5.6 * 10^{-14}$ to $10^{-10} \frac{m^2}{s}$

In particular, pore diffusion, a type of solid diffusion, is a crucial parameter for applications such as catalytic reactors and adsorption processes. Pore diffusion itself is divided into three categories of pore diffusion: Bulk diffusion, Knudsen diffusion, and surface migration. Bulk diffusion involves the diffusion of gas or liquid molecules through macropores (> 50 nm). Knudsen diffusion applies to the diffusion of gases through large cylindrical pores called mesopores (2-50 nm), which is of interest when considering the use of MOFs for safe storage of hydrogen to be later used in a fuel cell. Surface migration applies to micropores (< 2 nm) that is a representation of what occurs in diffusion of a solute through a bulk solid.<sup>5</sup>

Hindered solute diffusion in solvent-filled pores applies when a solute in a liquid solution is diffusing into tiny capillary pores (50 to 200 Å)<sup>6</sup> in a porous material. It is called this due to the hinderance provided by the pores themselves and the pore walls. The diffusion coefficient that describes this model is a function of the diffusion coefficient of the solute in an infinitely dilute solution and two reducing correction factors. Each correction factor is a function of the reduced pore diameter which is a ratio of the solute molecular diameter and the free pore diameter. These correction factors are bound by the principle that if the molecule was larger than the pore then it will not diffuse into it. This is ensured because as the reduced pore reaches one, the correction factors approach zero resulting in a diffusion coefficient of zero. The first correction factor is known as the steric partition coefficient which is based on geometric considerations of the solute particle trying to diffuse and is described by the equation:

$$F_1(\phi) = (1 - \phi)^2 \quad (2)$$

The second correction factor is known as the hydrodynamic hindrance factor which is based on hindered Brownian motion of the solute within the pore and is described by the equation:

$$F_2(\phi) = 1 - 2.104\phi + 2.09\phi^3 - 0.95\phi^5 \quad (3)$$

The other major type of solid diffusion involves diffusion into a bulk solid. This type of diffusion is more commonly known and is prominent in many processing techniques such as carburizing and nitriding. Solid-solid diffusion, within the bulk, is also what causes segregation of metal ions within a material which can lead to failure of a part such as when chromium diffuses to the surface of a steel and is all used up when it oxidizes at the surface and thus cannot be used any longer to protect the steel.<sup>5</sup>

## 2.2 Residence Time Model

Residence Time of a system is the amount of time that a single molecule of sorbent lingers in a reactor system before being purged. The residence time distribution (RTD) is the profile of a molecule leaving the system with the amount of time that a molecule can spend inside.<sup>7</sup> Residence time is needed in order to understand the mixing within reactors to determine how the real reactor that is being used compares to an ideal model. Often the RTD model can help to determine individual reactor models which can then be placed in series.<sup>8</sup> Using reactors in series can help to obtain the desired yield, size, and timescale. Overall the RTD can help to construct future reactors and understand any problems in the ones currently being used.

Different reactor types have different models for RTD. Continuous Stirred Tank Reactors (CSTR) and Plug Flow Reactors (PFR) are typical reactors that are used. CSTR reactors are unique because their concentration gradient of a species is the same both in and out of the actual reactor.<sup>8</sup> PFR reactors are slower but are much more efficient at converting all of the reactants as all species are converted before actually continuing in the system. Sizing becomes an issue with using only PFR reactors and a combination of them typically leads to a more ideal system based on both timescale and size.<sup>9</sup> PFR reactors have no mixing within them while CSTR reactors are typically assumed to be well mixed which means that it can be continuously run if complete conversion is not required or if the reaction is significantly spontaneous and quick.<sup>8</sup> The flow in the reactors have different dispersion models which dictate the residence time in the system. PFR reactors have no axial dispersion and are restricted in one direction until the yield is achieved and the products are released downstream.<sup>7</sup> CSTR has axial dispersion as it is mixed and leads to a residence time that follows an exponential decay.<sup>8</sup> Figure 3 shows the difference in the models.

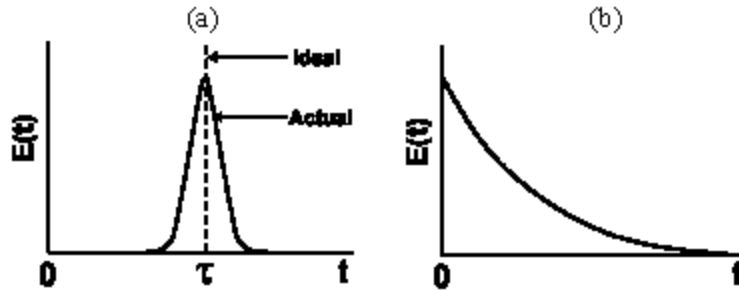


Figure 3: Concentrations using impulse input into PFR (a) and CSTR (b)<sup>8</sup>

The equations for finding the RTD are based on two different models. The Cumulative Distribution Function  $F(t)$  and the RTD Function  $E(t)$ . The cumulative distribution function is the model of the molecules that are exiting the reactor and have spent time in the reactor. The derivative of this function finds the RTD Function  $E(t)$  which is the amount of molecules that have spent a range or distribution of time in the reactor. The reason for using one or the other is determined based on the experiment that is chosen for finding the resonance time. The two options are pulse injection or the step method. Equations (4) and (5) are the RTD Function Equations for PFR and CSTR.<sup>8</sup>

$$E(t) = \sigma(t - \tau) \quad (4)$$

$$E(t) = \frac{1}{\tau} e^{-\frac{t}{\tau}} \quad (5)$$

The RTD of PFR and CSTR reactors can be found by using one of two methods. A pulse injection can be used to directly determine the  $E(t)$  equation which has benefits in losing error in taking the derivative of  $F(t)$ .<sup>7</sup> It is useful if the material is expensive and a pure stream cannot be used through the system. Steps have an abrupt change from a concentration of zero to a maximum concentration. The step method is easier to perform but is more difficult to model  $E(t)$  based on the results. Figure 4 shows the method and the responses for both pulse and step injections.<sup>8</sup>

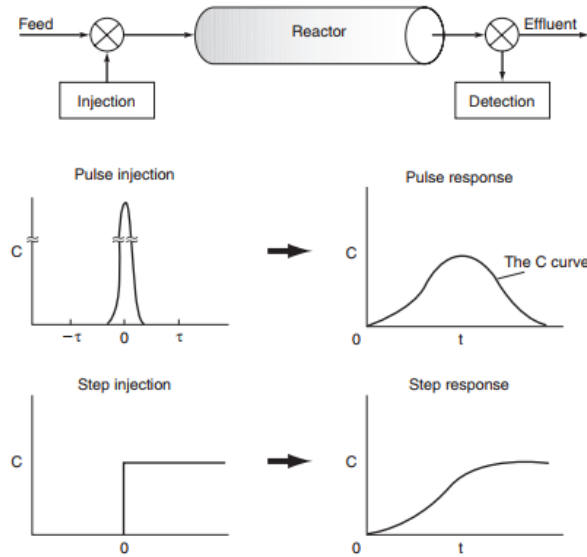


Figure 4: The Methods of Pulse and Step Injections and their Responses<sup>8</sup>

A benefit of the modeling of RTD is the diagnosing of dead volume in a system. When conducting experiments, the dead volume can lead to inefficiencies and can lead to holdup in the release of all species in the system. In order to know how much is in the system, residence time ( $\tau$ ) is equated to the dead volume over the volumetric flow rate.

$$\tau = \frac{V}{v_o} \quad (6)$$

By finding this, a systematic removing of pieces of the system can be conducted in order to reduce the dead volume to an acceptable value for the experiment. In a cell that was used in one experiment, multiple steps with different flow rates were taken using a high-performance liquid chromatography machine.<sup>10</sup> By finding the residence time at each flow rate and plotting versus the inverse flow rate, the dead volume of the system can be found.<sup>11</sup> RTD is used in this project to optimize the high-performance liquid chromatography system to reduce its effect on desorption profiles in a reactor bed. The desorption profile tends to be affected by washout time in the short-

time profile and a reduced dead volume means that the system does not need to run longer times, thus saving time and material.

### 2.3 High Performance Liquid Chromatography (HPLC) System and Uses

A high-performance liquid chromatography (HPLC) is a machine designed for the flowing of liquids at a specific flow rate through different flow modules until it ultimately reaches a diode array detector (DAD) that is used for sampling. The typical setup involves the two binary pumps that pipe to a degasser for pure liquid solutions and no gas that can damage the detector. These binary pumps then connect to two mixing points to ensure that the flow is consistent and well mixed, which allows for a removal of any previous contaminants. From the mixing point, the flow travels to an injector port where sorbate can be added by an automated micro-injector or in the use of step methods. The injector port is important for insertion of pulse slugs that can be characterized through a column or could be used to find residence times in a reactor. From here the flow goes to another six-port valve that can send the flow through a column. From here it goes to the DAD and is purged out of the system to waste.<sup>12</sup>



Figure 5: HPLC Setup

The HPLC's use of columns is the main advantage to using an HPLC. The columns can be used to separate an unknown mixture from an injected pulse or a flow from a large amount of liquid.<sup>13</sup> Different types of columns can be inserted, but the typical system has a column packed with resin that chromatographically separates the components into different fluid slugs that then travel at different points through the detector and a range of wavelengths can be used to determine the flow's composition.<sup>14</sup> The high pressure in the system is needed to force the slugs through the column and differentiates the system from a regular liquid chromatography what simply looks at single species sorbates. Figure 6 shows the basic setup for an HPLC system.

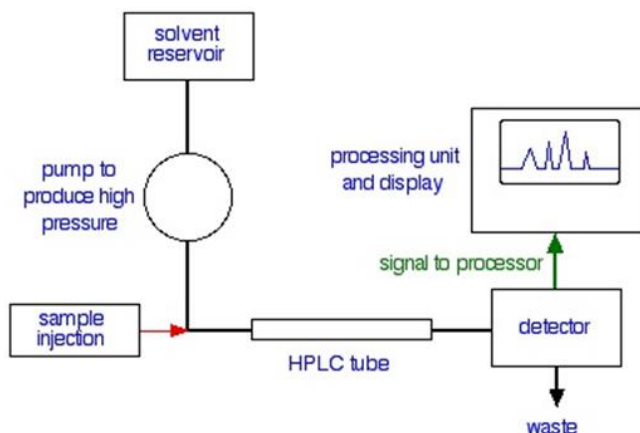


Figure 6: HPLC schematic showing how a solvent reservoir gets pumped through a high pressure pump to sweep the sample injection through an HPLC tube to the UV detector.<sup>15</sup>

The system is often compared to gas chromatography (GC) due to their use in separations and characterizations. While GCs use an inert carrier which does not differ very much between different samples, HPLCs need specific solvents in order to run between different solutions. Sometimes water would be needed for inorganics and an alcohol might be needed for organics. The type of columns also makes a large difference. In HPLCs, a tight packed column must be used while the GC can use capillary columns or tight packed ones.<sup>16</sup> Capillary columns typically have better resolution of separations. Ultimately the choice between the two machines comes from the use of volatile mixtures that are flowed as the sorbate. HPLC needs a liquid mobile phase.<sup>17</sup> The use of liquids offers a better way to understand solutions than trying to gasify all components for use in a GC. In the system analyzed in this report, the analyte is paracetamol, which is non-volatile, so HPLC was the ideal mechanism for data collection.

The DAD in HPLC systems typically have a tungsten lamp that emits visible light which goes through a deuterium lamp to add more wavelengths of light along with some portions of the UV spectrum.<sup>18</sup> The light passes through a slit and onto a diffraction grating to split the light into various wavelengths. Another slit enables the desired specific wavelengths to pass through and

this grating is moved depending on what is needed.<sup>18</sup> The light then passes through a flow cell and then through a photodetector after going through the fluid and the difference in the amount of light supplied and received is measured in absorbance units (AU).<sup>12</sup> Figure 7 shows the process.

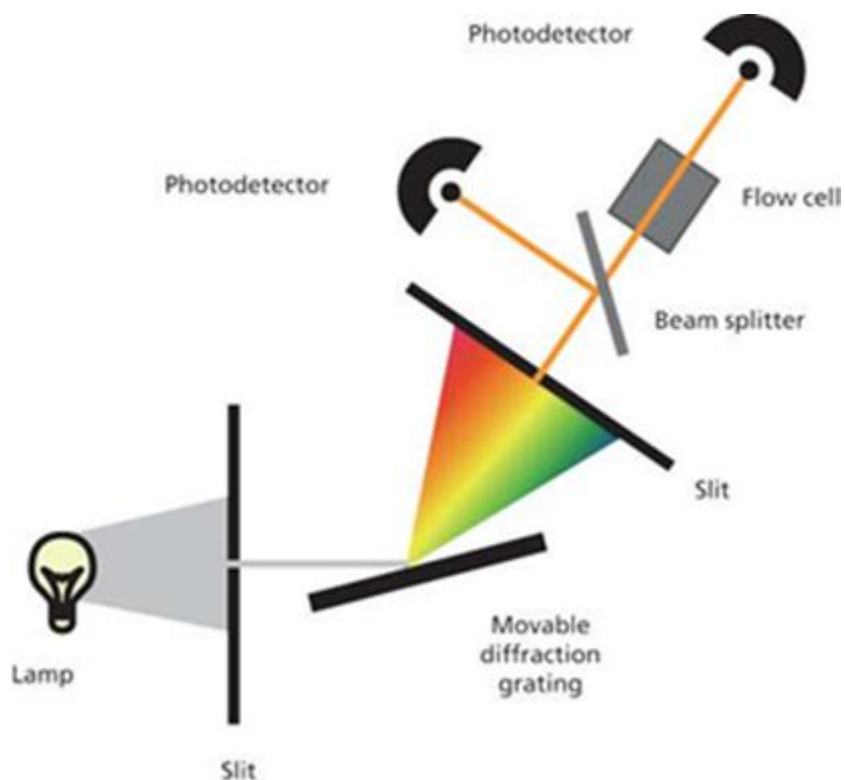


Figure 7: Diode Array Detector Schematic. Light from the lamps travel through a slit to be diffracted into a slit that can be moved depending on the wavelength needed. This beam is then split for a reference and allowed to go through the flow cell to another detector that shows the resulting intensity.<sup>19</sup>

## 2.4 Zero-Length Column Modeling

Zero Length Column (ZLC) analysis is used to determine the adsorption and desorption characteristics of certain materials. ZLC is typically used for gas phase, but the same concept applies to liquid phase (with minor mathematical model adjustments). A basic ZLC apparatus includes two feed streams (one pure solvent, and one with a known concentration of sorbate/analyte). These two feeds enter a valve that can switch between them. The valve pipes to a column of “zero-length”, or a very small length, which allows for the assumption of a well-mixed

cell. The ZLC is packed with a very thin (1 particle thick) fixed bed of sorbent. A general process of the ZLC can be seen below in Figure 8.

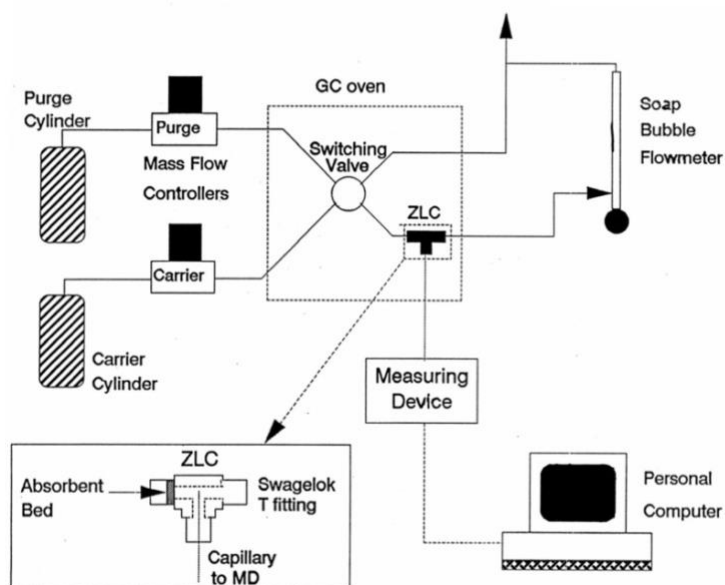


Figure 8: Basic ZLC Apparatus showing all general parts and basic flow pattern. <sup>20</sup>

A



B

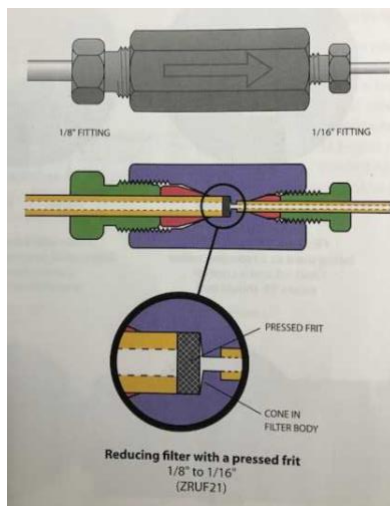


Figure 9: Image A shows the ZLC Column used in this project with 1/16th inch tubing going to a 1/8<sup>th</sup> expander which is fit to the chamber at the two frits. This is then reduced on the other side downstream. Image B shows the ZLC model and all parts were purchased from Vici Valco.

The Péclet number ( $Pe$ ) is the ratio of the advective transport rate to the diffusive transport rate ( $Lu/D$ ), which also describes the axial mixing within a packed column (a larger  $Pe$  means better axial mixing). With this definition, as the length,  $L$ , approaches 0,  $Pe$  approaches infinity. In gas phase ZLC, a small sample of absorbent is brought to equilibrium with a sorbate at a known partial pressure. After the column, the effluent flows through a detector that reads the concentration of the sorbate. The sorbate is transported by an inert gas, typically helium. At the start of the experiment, the feed to the column is switched by the valve from the pure carrier stream to the stream with a known partial pressure of the sorbate in the carrier. The detector produces a response

curve in terms of the concentration of the sorbate over time. Changing system components like pressure, temperature, flow rates, etc. will elicit different response curves.

Ruthven & Stapleton used a ZLC to model the desorption characteristics of Zeolite-NaX. In this paper, it was determined that the ZLC was dependent on following the transient desorption curve with a small amount of the zeolite crystal packed in the column. The system in this experiment consisted of benzene (sorbate) in hexane. Initially, the zeolite was saturated with the sorbate. Once saturation of the zeolite was achieved, the flow was switched to pure hexane at a relatively high flow, effectively removing the sorbate.

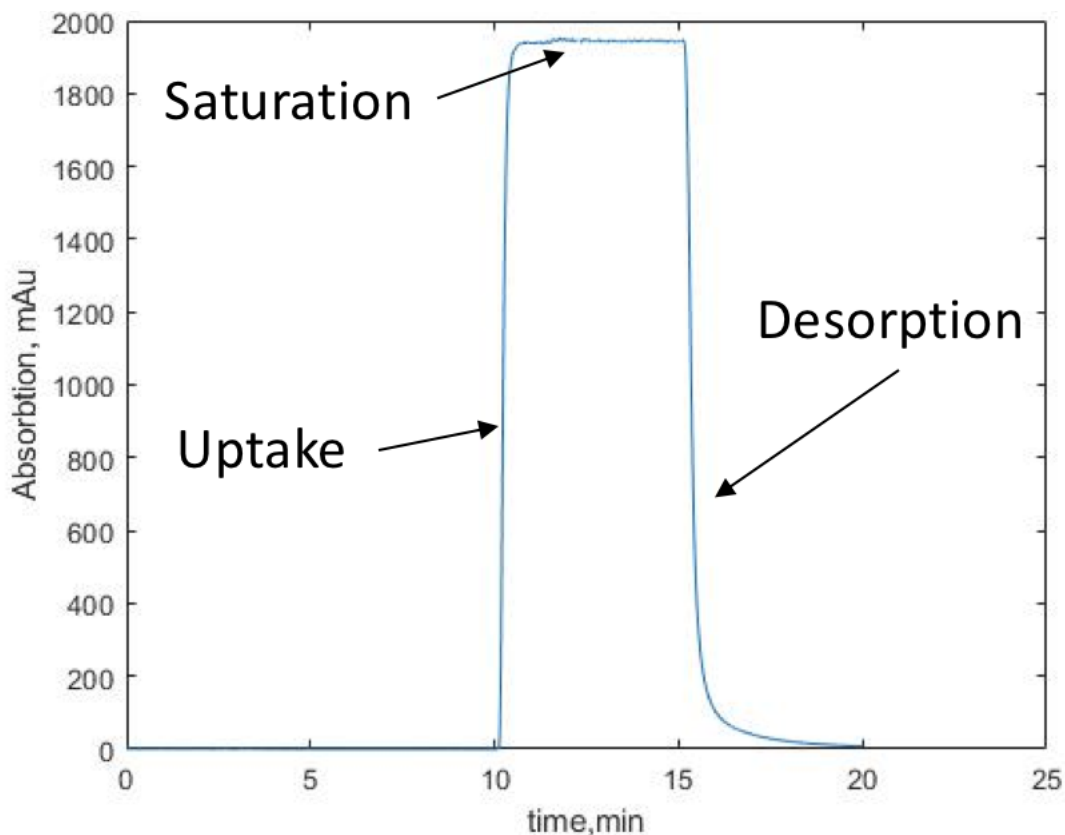


Figure 10: Full uptake, saturation, and desorption profiles

The desorption rate was controlled by the internal diffusion of the crystal. Therefore, the external concentration of the crystal must remain at zero, which necessitated the aforementioned

relatively high flow rate. Although this process of liquid phase ZLC is very similar to the equivalent gas phase, mathematical modeling of the liquid phase becomes more involved.<sup>21</sup>

## 2.5 Mathematical Model

Brandani and Ruthven wrote many papers that were useful in the mathematical modelling of the desorption curve for a ZLC with liquid systems. The paper describes an approach to experimental data in regards to a binary liquid system through a zeolite absorber. The model is based on an analytical method that is controlled by intraparticle diffusion. This means that the model takes into account the time constant for diffusion between the sorbent and the washout time for the desorption of the sorbent. The derivation of the model begins with two mass balances, one on the fluid phase of the flow and one on the solid phase. The solid material (phase) is typically a zeolite. When time is zero, the initial concentration is defined by a constant. The boundary conditions are defined at the center of the particle and at the surface of the particle for the solid phase mass balance. The solid phase balance is then inserted into the fluid phase balance to simplify the equation. Through changing variables like diffusivity and noting that there will be a finite amount of adsorbed paracetamol at the surface of the particle, the correct boundary condition at the surface is determined to be non-zero and can be solved for numerically. Equation (7) through (13) shows the important equations in used in the process of solving the mass balances.<sup>22</sup>

Governing Equations:

Fluid-phase mass balance:

$$V_s \frac{d\bar{q}}{dt} + V_f \frac{dc}{dt} + Fc = 0 \quad (7)$$

Solid-phase mass balance:

$$\frac{\partial q}{\partial t} = D \left( \frac{\partial^2 q}{\partial r^2} + \frac{2}{r} \frac{\partial q}{\partial r} \right) \quad (8)$$

Initial Conditions:

$$q(r, 0) = q_0 K c_0; \quad c(0) = c_0 \quad (9)$$

Boundary Condition:

$$\left( \frac{\partial q}{\partial r} \right)_{r=0} = 0 \quad (10)$$

Equation (7) can be considered as a boundary condition on the solid-phase mass balance (Equation (8))

$$\frac{4}{3} \pi R^3 \frac{d\bar{q}}{dt} = 4\pi R^2 D \left( \frac{\partial q}{\partial r} \right)_{r=R} \quad (11)$$

With equilibrium at the surface;

$$q(R, t) = K c(t) \quad (12)$$

Separation of variables allows for the equation to be solved. The paper further simplifies beyond what is needed for a liquid system that is present in our methods. The gamma term that was set to zero cannot be zero in this case, due to the fluid being a liquid rather than a gas. This adjusts for liquid holdup in the system. In the creation of desorption curves, the long time is needed to ensure that the exponential decay will reach the  $\frac{R^2}{\beta_1^2 D}$  as the washout process is still going on. Equation (13) shows the concentration over shorter times and the tuning of L and gamma to be able to obtain the value of  $V_f$  and the diffusional time constant. These are obtained using the slope and intercept of the long-time asymptote with the graph of the short time.<sup>22</sup>

$$\frac{c}{c_0} \simeq 1 - \frac{LD}{\gamma R^2} t \simeq \exp \left( -\frac{F}{V_f} t \right) \quad (13)$$

A numerical solution, created in Matlab, solves Equation (8) as a boundary value problem using initial and boundary conditions defined in Equations (9), (7) and (10) respectively. The outer

boundary condition at the outer radius of the particle is solved for as a function of flow rate using Equation (7). The diffusivity value was estimated until the resulting desorption profiles fit the HPLC data, with emphasis on fitting the long-time desorption region.

The analytical solution was derived by Ruthven and Brandini as well.<sup>22</sup> This solution is based on gas phase in a ZLC. It makes several assumptions that are not valid for this project's system because it is liquid phase in a ZLC and the holdup term that is not used in the assumption would be required in this situation.

## 2.6 Zeolites

Zeolites are porous crystalline materials with large specific surface areas.<sup>23,24</sup> Typically composed of networks of aluminum and silicon tetrahedrally bonded to oxygen atoms ( $\text{Al}_2\text{O}_3$  and  $\text{Si}_2\text{O}_4$ ) that are connected by corner oxygen atoms, zeolites have a cage-like structure with many micropores. Zeolites may also contain positive cations, like sodium or potassium to balance out negative charges within the structure.<sup>25</sup> Pore sizes of zeolites tend to be between 0.3 nm and 2 nm. Due to the continuous microporous structure and high specific surface area of these materials, zeolites find uses in many different areas such as carbon dioxide capture<sup>26</sup>, catalysis<sup>27</sup>, and ion exchange<sup>28</sup>.

While a great supply zeolites exist in the natural world, many types are not suitable for many applications due to structural defects and chemical impurities.<sup>23</sup> Rather, synthetic zeolites are more commonly used when precision of structure is critical. These zeolites are more pure and have a structure more uniform than that of natural zeolites, and differences in temperature, pressure, reagent concentration, pH, and reaction period can be manipulated to form different kinds of zeolites.<sup>25</sup> These different kinds of zeolites are classified by the ratio of alumina to silica in their

structures. Low silica zeolites like Na-X have molar ratios of Si/Al less than 2. Intermediate silica zeolites like Na-Y have Si/Al ratios between 2 and 5, and high silica content zeolites like ZSM-5 have Si/Al ratios greater than 5.<sup>29</sup>

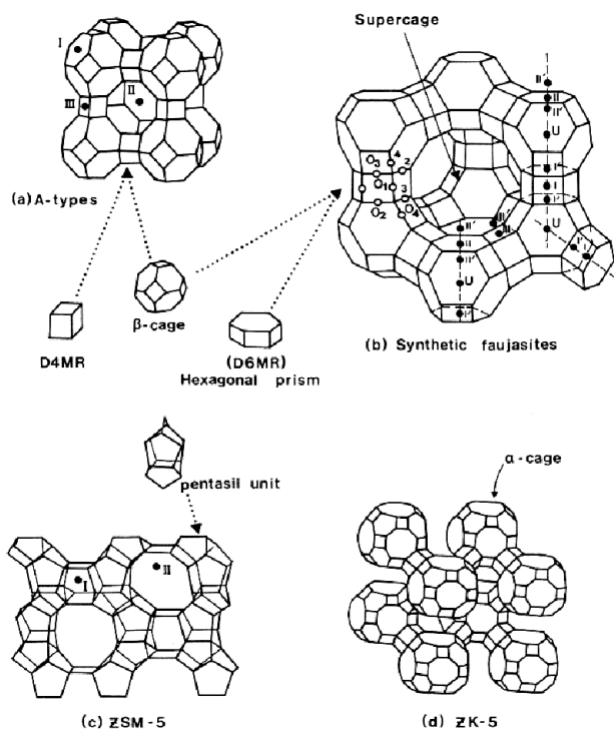


Figure 11: Different Cage Geometries of Various Zeolites. These different cage shapes result in different overall network structure with different pore sizes<sup>30</sup>

## 2.7 Metal Organic Frameworks (MOFs)

### 2.7.1 Characteristics

Much like zeolites, Metal Organic Frameworks (MOFs) are 3 dimensional microporous structures that have a uniform structure and high specific surface areas typically between 1,000  $\text{m}^2/\text{g}$  and 10,000  $\text{m}^2/\text{g}$ .<sup>2,31</sup> Unlike zeolites, which are composed largely of silica and alumina tetrahedrally bonded to oxygen atoms, MOFs are built from organic ligands bonded to metal ion clusters. These clusters are the secondary building units (SBUs) of the MOF and are one of the main differences between zeolites and MOFs.<sup>32</sup> These SBUs are important for stability of the MOF

and create permanent porosity. The connecting units between the metal clusters are organic ligands. Together with the SBUs, these ligands form rigid geometries like squares and octahedra that provide structural stability throughout the material.<sup>31</sup> These ligands are typically carboxylates, but tetrazolate and sulfonates can be used during MOF synthesis as well allowing for many of the chemical properties and physical pore dimensions to be highly tunable. This tunability allows for MOFs to have a range of pore sizes from several angstroms for microporous MOFs to nanometers for mesoporous MOFs.

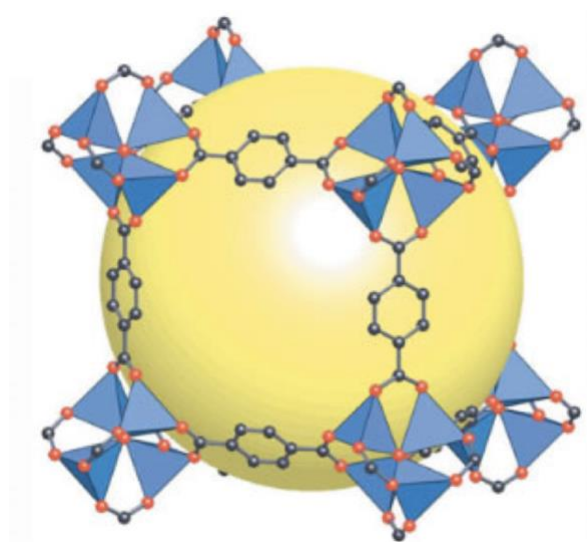


Figure 12: Basic MOF Structure (Red – metal atoms, Black – organic linker, Yellow – internal volume)<sup>33</sup>

In Figure 12 above, the red dots represent metal ions and the black dots represent organic linker molecules. The yellow space is the unoccupied volume inside the MOF pore, which is the space inside the cage created by the SBUs and organic linkers. The relative size of yellow space compared to the ion clusters and linkers shows how large the pores are compared to the materials they are composed of.

MOFs have very high specific surface area due to their high porosity (typically higher than 50% of the total volume)<sup>31</sup>, making them suitable in many different applications like catalysis, gas capture, and drug delivery. This high surface results in a large amount of space for adsorption to the MOFs surface. The amount of material that can be stored per a certain mass or volume is an important factor in drug delivery, gas storage, and capture. For example, CO<sub>2</sub> capture is a technique used to reduce greenhouse gas emissions to the atmosphere from industrial processes. CO<sub>2</sub> adsorbs to the surface of the MOF, preventing it from being released into the atmosphere. Getting the most CO<sub>2</sub> captured per unit mass or volume is critical to reducing emissions and maximizing capture due to restraints of the operational equipment, and MOFs are suitable materials for the job. MOFs MIL-101 and MOF-107 have great potential in these applications because they have been found to capture 40 mmol of CO<sub>2</sub> per gram of MOF and 33.5 mmol of CO<sub>2</sub> per gram of MOF, respectively.<sup>2</sup> MgMOF-74 also shows great potential as a CO<sub>2</sub> capture material. Compared to other high surface area materials like zeolites, MgMOF-74 was able to capture more than twice as much CO<sub>2</sub> as other MOFs and zeolites tested.<sup>34</sup>

The high adsorption capacity of MOFs is also important in drug delivery since more of a drug can be contained in a smaller space. Additionally, the materials MOFs are composed of are non-harmful and the linkers can be chosen so that they are biodegradable and minimize harmful side effects to the body.

### 2.7.2 History of MOFs

The many applications of porous materials like zeolites has been the focus of many different fields since the 1800s. However, the materials that they are composed of as well as the chemical techniques that are used to synthesize zeolites limit the control over the final zeolite structure. This limitation led to great interest in finding a method to create fully controllable and

tunable microporous structures and materials that could be used in similar applications as zeolites. The result of this research was the synthesis of MOFs. The first MOFs appeared in the early 1990s, with the term MOF being used for the first time in 1995.<sup>35</sup>

The first significant early MOFs were reported in two publications in 1999. Ian Williams published an article on HKUST-1 MOF in March of 1999, while Yaghi published on MOF-5 in November.<sup>35</sup> These were two of the first publications to mention highly porous MOFs with large specific surface areas. In particular, MOF-5 showed higher specific surface area than most zeolites. Since the explosion of MOF research in the 1990s, more than 20,000 types of MOFs have been synthesized.<sup>31</sup> One of the most important discoveries in the last couple of decades involves the structure of MOFs and how they differ from other coordination structures. Many coordination compounds were composed of organic linkers such as 4,4-bipyridine connected by metal ions. Eventually, coordination compounds created in this way suffer from a collapse of structure and destruction of the pore. The discovery that using multidentate linkers like carboxylates allow metal ions to create M-O-C clusters was significant in creating MOF structures with permanent porosity.<sup>32</sup> Figure 13 shows the difference between a coordination compound made of an N-bound polytopic organic linker like 4,4-bipyridine and one with secondary building units.

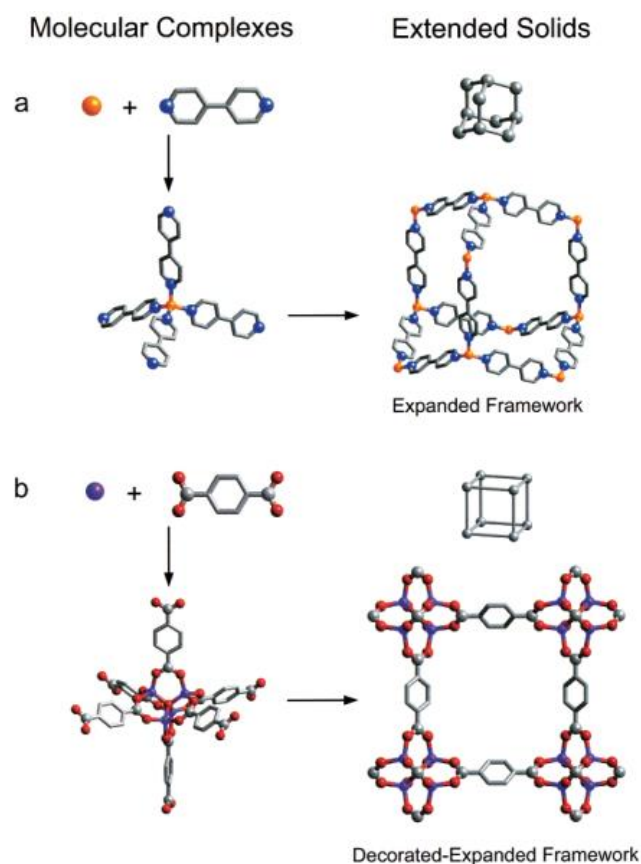


Figure 13: Older coordination compound (a) vs MOF structure with SBUs (b)<sup>32</sup>

These SBUs lead to a more stable structure with in turn leads to permanent porosity, or pores that do not break down as a result of broken structure. Permanent porosity was a desirable property poised by zeolites that was now able to be synthesized in synthetic MOFs.

The synthesis of higher surface area MOFs has been difficult due to the fact that multiple frameworks that became intertwined seemed to form when using longer organic linkers (longer organic linkers are required for ultraporous MOFs).<sup>31</sup> This problem was solved by selecting certain linkers that prohibited the construction of multiple internal frameworks by using materials that create MOFs that would have to form a different topology in order to create interpenetration. In 2004, this approach yielded the highest surface area MOF ever created with 3780 m<sup>2</sup>/g, and

within 6 years that milestone was nearly doubled in 2010 when a MOF with 6240 m<sup>2</sup>/g and 90% porosity was synthesized.<sup>31</sup>

### 2.7.3 MOF Synthesis

The basic MOF synthesis materials consist of the metal in salt form, the organic linker molecule, and a solvent for the crystallization to take place in. The metals are typically zinc or copper salts. The organic linker molecules have carboxylic acid groups on either end to serve as a bonding site to the metal ion. The solvent used in the crystallization process is a formamide solvent, typically dimethylformamide or diethylformamide.

The classical solvothermal synthesis involves mixing the metal salt with the organic linker in a stable solvent. This solution is put into a pressure bomb and heated to catalyze the crystallization process. Once the crystallization is completed, the reaction is quenched in room temperature water and the crystals are extracted. The advantage of this process is the simplistic equipment. One disadvantage is the lack of repeatability.

While MOFs are typically synthesized solvothermally, there are studies that show more reliable, and stronger yield syntheses. One synthesis method that has been studied more recently is the use of ultrasonic irradiation. Ultrasonic irradiation can lead to homogeneous nucleation. This would be desirable if the product required needed to be uniform in structure. Another main difference between ultrasonication and other methods of synthesis is the acoustic cavitation phenomenon. This is the creation, growth, and collapse of a bubble in a liquid medium. This phenomenon leads to extremely high localized temperatures, on the order of 2000K - 5000K, very high cooling rates, and shockwaves created by the homogenous cavitation. This dramatically changes the surface morphology, composition, and reaction rate of the then produced crystal.

Another crystal synthesis route is microwave radiation. Microwave radiation is much more commonly used in large scale production and produces a more desirable crystal due to the direct

and uniform energy of the microwave system. Microwave radiation also leads to homogeneous nucleation like ultrasonication, and also leads to fast crystallization, diverse morphology and size, phase selectivity, and particle size.

With the vast difference in types of MOFs and their respective syntheses, characterization methods are required to compare the crystals. Some of these characterization techniques include x-ray diffraction, fourier-transform infrared spectroscopy, thermogravimetric analysis, and Brunauer-Emmett-Teller analysis.<sup>2</sup>

#### 2.7.4 IRMOFs

A widely studied class of MOF is that of isorecticular MOFs (IRMOFs). IRMOFs share a common cubic structure, with zinc vertices connected by organic linkers. These MOFs can be synthesized in many different ways, but most commonly they are synthesized in a solvothermal procedure, where a zinc salt and the organic linker are dissolved in a formamide solvent.<sup>2</sup>

#### 2.7.5 MOF Imaging

Nanoscale MOFs (NMOFs) can serve as molecular imaging probes. One type of imaging these compounds can be applied in is optical imaging. This type of imaging is common during surgeries and allows for great improvement in the outcome of the surgery. Currently, conventional fluorophores and quantum dots are utilized for this application. Inherently luminescent NMOFs don't make the cut when it comes to the required absorption and quantum yields needed to effectively image something like an organ or tissue. For this reason, many of these NMOFs are functionalized with various dyes to improve these yields. Rowe *et al.* prepared Gd(III) NMOFs that were functionalized with polymer chains that contained fluorescein. These NMOFs were used to target cancer cells and the showed specific location of these cells after 1 hour of incubation and 24 hours of internalization. Another group developed Gd(III) NMOF particles where the organic linker was functionalized with perylene-3,4,9,10-tetracarboxylate, which is an anionic dye. Both,

*in vitro* and *in vivo* experiments revealed good biocompatibility and accumulation of the NMOF in the liver. Lin *et al.* functionalized an Fe-based NMOF with a Bodipy-based fluorophore which was not fluorescent due to iron quenching. However, it was fluorescent when the MOF began to break down.

Even though optical imaging can provide excellent resolution, the natural luminescence of tissue and ingested compounds can make it difficult to quantify the fluorescence signals that are being provided by the NMOF. Also, the penetration depth is limited. These drawbacks can be limited though by optimizing the combination of mode of imaging and contrasting agent. Also, regardless of these drawbacks, this type of imaging is fast and optimal for high-throughput screening meaning that it can be used for *in vitro* cell labeling.

Another type of imaging where these NMOF systems can be utilized is magnetic resonance imaging (MRI). This technique is a noninvasive diagnostic method for providing high quality images of internal structures of the body. The contrast that is developed by MRI is a result of differences in the relaxation rate between tissue water photons. This contrast can be greatly improved by using a contrasting agent which essentially decreases the relaxation rate of the photons. The effectiveness of the scan depends on the positive and negative enhancement. Based on the positive and negative enhancement signals acquired, contrasting agents are categorized under T<sub>1</sub> or T<sub>2</sub> binary types. Currently available T<sub>1</sub> contrasting agents include Gd-related complexes due to their paramagnetic properties. Currently available T<sub>2</sub> contrasting agents are mostly nanoparticles which include superparamagnetic iron oxide. Recent research has looked to use NMOFs for the purpose of carrying large amounts of paramagnetic ions. Lin *et al.* created NMOFs that incorporated Gd<sup>3+</sup> ions into the center of each which demonstrated exceptionally large positive and negative enhancement since there was such a large concentration of Gd<sup>3+</sup> ions.<sup>36</sup>

## 2.8 MOF Applications

### 2.8.1 Drug Delivery

Chemotherapy is still the most common treatment method for cancer. Chemotherapy brings upon negative side effects and a low chance of succession for certain cancers. Traditional direct drug administration is not as effective either as this mode causes negative side effects and poor drug distribution in the body. Some newer technologies include liposomes, nanoemulsions, nanoparticles and micelles which allow more directed drug delivery. However, these compounds suffer from low loading capacities and porous inorganic compounds themselves have undesirable toxicity and degradability once inside the body.

Drug carriers in general require these properties:

- Hold a high “payload”
- Controlled release without demonstrating the “burst effect”
- Control the degradation of the matrix
- Easily engineer surface in order to control *en vivo* fate
- Characterize by imaging techniques

MOFs provide an excellent match to the required properties. The advantages of using MOFs for drug delivery is due to their structure, morphology, composition, pore size, and chemical properties can be manipulated to allow for stimuli-controlled drug release and functionality. MOFs’ high surface area allowing for them to have high “storage” capacity. Lastly, the presences of organic linkers allow for them to be easily biodegradable within the body.<sup>3</sup>

Férey et al. developed two chromium-based MOFs to study the desorption kinetics of IBU, a non-inflammatory drug, to see if the use of these MOFs would be suitable for the delivery of this drug. However, chromium is known for its toxicity to the human body so Fe-based MOFs were developed as well.<sup>37</sup> The iron-based MOFs reported a 21-day total release time for IBU when

tested in a simulated body fluid at 37°C. These MOFs also showcased an ability to adapt their pore size to the size of the molecule to maximize the drug-matrix interactions. The Fe-based MOFs were also tested with other drugs such as the antitumor drug DOX and antiviral drugs CDV and AZT-TP where they continued to show high loading capacities for these drugs.<sup>3</sup>

Zn-based MOFs were also being tested as nanocarriers for the anticancer drug 5-Fu and the antitumor drug RAPTA-C. The Zn-based MOF utilized for delivery of 5-Fu showed a total release time of 7 days. Figure 14 shows this release data collected by C. Sun *et al.*, but mechanisms for release nor manipulation of pore size was not tested in this study.<sup>38</sup>

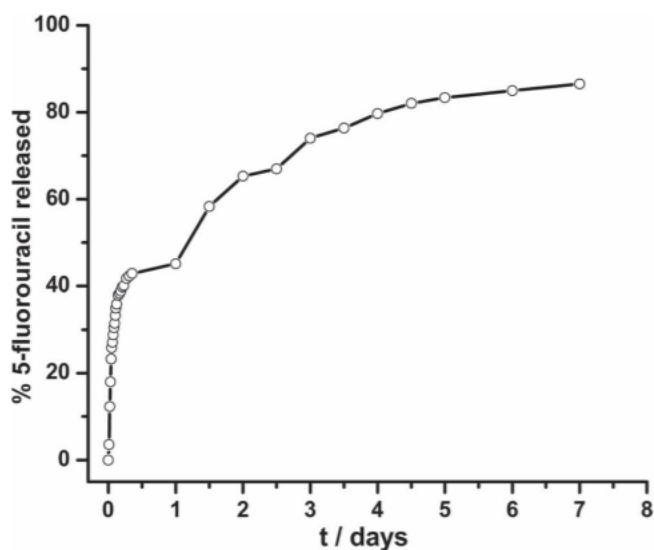


Figure 14: 5-Fu Release Profile for a Zn-Based MOF<sup>38</sup>

A second group, S. Rojas *et al.*, prepared a second type of Zn-based MOF that had four different derivations. These derivations utilized four different side groups (-OH, NH<sub>2</sub>, H, and NO<sub>2</sub>) on the organic linker to see how the side group affected the release profile. These MOFs showed release times in between 49 to 80 days as partially shown in Figure 15. However, there was an initial burst release observed for all four MOFs. It is summarized that the -OH derivative MOF shows higher delivery rate due to possible degradation of the MOF matrix. The -NH<sub>2</sub> derivative

shows a slower release but still it is high and this may be due to the polarity induced by the side group causing the MOF to essentially hold onto the RAPTA-C molecule more strongly as well as having a smaller pore volume than the other MOFs. The step delivery profile is possibly due to matrix flexibility. The -H and -NO<sub>2</sub> derivatives show controlled, slow, and linear release profiles and this may be due to high loading capacity of the -H derivative and small polarity exhibited by the two side groups.<sup>39</sup>

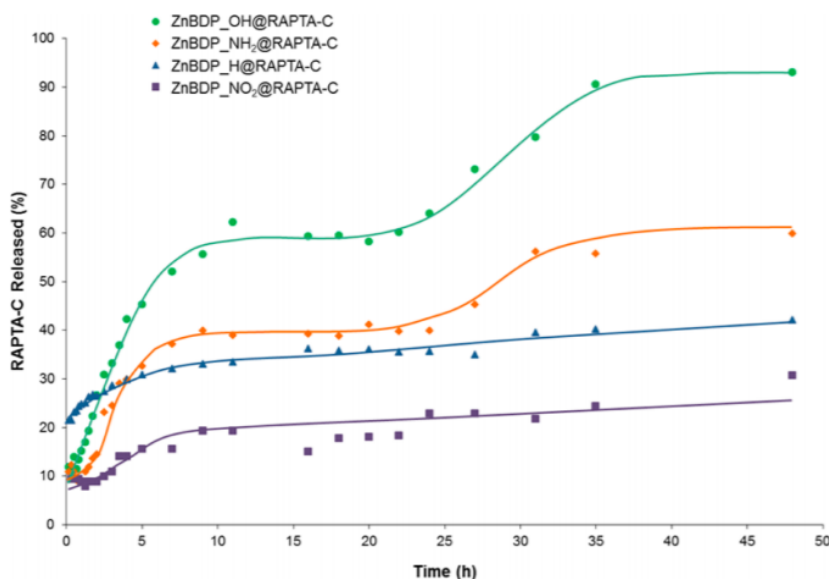


Figure 15: RAPTA-C Release Profiles for Four ZnBDP MOFs<sup>39</sup>

Zr-based MOFs are of special interest in the use of drug delivery due to their two octahedral and tetrahedral cages, high stability, and non-toxicity. Lin *et al.* studied the use a Zr-based MOF for the encapsulation and coordination of a cisplatin prodrug and siRNA. This resulted in the apoptosis of the targeted cells in the experiment meaning that this co-delivery method would improve the effectiveness of the chemotherapeutic effects of cisplatin *in vitro*.

Some MOFs are also stimuli responsive. One such stimuli that promotes drug release is pH. An example of this was an Fe-based MOF in which a layer of silica was deposited on the surface of the MOF. The MOF, independent of the coating, readily released the drug upon entering

an environment with a low pH. To allow for a slower release, the silica coating was applied to the MOF. A second response is a magnetical response. A common material that MOFs are being composed of for this task is magnetite (Fe<sub>3</sub>O<sub>4</sub>). The interesting part about this type of response is that these MOFs can be magnetically guided to the site of the tumor to allow for more effective therapeutic results. A third type of stimuli-responsive MOF is one that is sensitive to small changes in the physiological temperature of the human body. One example of this involves using PNIPAM as a building block in the MOF. This is because PNIPAM has a cloud point around 32°C and thus when the temperature of the system the MOF resides in goes below this temperature, PNIPAM becomes hydrophilic and will dissolve in water, but, in the process, will also form an aggregate. This dissolution in water allows for drug release and so sicknesses that cause variations in the temperature of the body will cause release of the drug until the temperature stabilizes.

Since the human body is a complex organism, using MOFs with a single stimuli response may not be sufficient. To address this issue, the development of multiple-stimuli-responsive MOFs is being carried out to further increase the precision and efficacy of drug delivery. One supramolecular host that is quickly becoming applicable for this task is a pillararene. Pillararenes possess a special structure that allows for excellent host-guest performance and versatile functionalization. Pillararene-based structures have been proven to act effectively as nanovalves. This function. One such group developed a MOF-nanovalve system where UMCM-1-NH<sub>2</sub> acted as the host material and was modified with carboxylatopillar[5] arene (CP5) that is linked with positively-charged pyridinium stalks. When this system enters an acidic tumor cell or tissue, the CP5, which acts as the gatekeeper, will experience a weakening of the noncovalent bonding between itself and the pyridinium stalks. This weakening leads to an “opening” of the nanovalve and thus the MOF will now be unblocked to the environment and will release the molecules it

stored. This system showed negligible premature release, negligible toxicity, biodegradability and biocompatibility. Another system developed is based on CP5-gated Zr-MOFs to provide a tri-stimuli-responsive effect. The three stimuli are low pH and increasing temperature which weaken the noncovalent bonds between CP5 and the stalks with the third stimuli being competitive binding since CP5 has a higher binding affinity for  $\text{Ca}^{2+}$  than for the stalks it is originally bound to. This system shows promise for future use in bone cancer therapy and bone regeneration as it showed controlled drug release in surroundings similar to that in osteoclasts and tumor cells which are generally low in pH and have high  $\text{Ca}^{2+}$  concentrations. These responses in conjunction with the high temperature response give it desirable properties and performance. Another supramolecular host that is of interest is  $\beta$ -cyclodextrin ( $\beta$ -CD). It also works as a sort of “gatekeeper” and can be tethered to most MOFs. Zhang et al. developed a system where they functionalized an Fe-based MOF with a  $\beta$ -CD derivative and peptide-functionalized polymer and encapsulated the drug DOX. This drug carrying system possessed pH- and redox-responsiveness and when tested on tumor and cancer cells it showed high uptake into the tumor cells and efficient drug delivery. Wang et al. also developed a system where they tethered  $\beta$ -CD to the surface of the MOF UiO-68-azobenzene. The azobenzene group is able to change its isomer arrangement from cis to trans and vice-versa when exposed to light. The cis/trans isomerization, and more specifically the one of trans to cis, promotes the dethreading of the  $\beta$ -CD molecules and allows for delivery of the drug. It was also found that the compound amantadine promotes competitive binding due to the higher binding affinity that  $\beta$ -CD has for amantadine causing dissociation of  $\beta$ -CD from the azobenzene stalks and thus, release of the drug.

### 2.8.2 Pesticide Detection and Concentration

There exists a major and continually growing concern for the health and safety of the public and the environment when it comes to the dangers regarding pesticides. Organophosphorous pesticides (OPPs) account for a large portion of concern due to its widespread use worldwide. OPPs are used for herbicides, insecticides, fungicides, and sprout inhibitors. These OPPs have all been used to increase agricultural output.

Currently, methods to detect the presence of OPPs are limited to characterization techniques based on chromatography. These methods require expensive equipment, which is not always widely available. In X. Xu *et al*, ZnPO-MOFs were synthesized to be used as a much cheaper alternative to detect the presence of one particular toxic pesticide. The luminescent ZnPO-MOF studied in this paper has its fluorescence intensity quenched when in the presence of a pesticide. As the pesticide is absorbed into the MOF, the fluorescent activity is decreased at a predictable rate. The pesticide concentration was measured by observing the fluorescence intensity of ZnPO-MOF at various amounts of the OPP parathion-methyl. These responses were plotted against a titration curve of the MOF in the presence of parathion-methyl to observe the quenching efficiency as a function of the logarithmic concentration of the pesticide. In a real sample, this MOF was able to detect the concentration of the parathion-methyl with relatively high accuracy. ZnPO-MOFs demonstrate a very wide range of detection of pesticides ( $1.0 \mu\text{g kg}^{-1}$  to  $10 \text{ mg kg}^{-1}$ ) with a lower detection limit of  $0.12 \mu\text{g kg}^{-1}$  for parathion-methyl. This high efficiency can be attributed to MOFs excellent adsorption ability to the analyte.<sup>36</sup>

### 2.8.3 Anti-Corrosion Coatings

MOFs have been recently investigated for their potential anticorrosion characteristics. MOFs that are highly water stable and hydrophobic MOFs are good contenders for anticorrosion coatings. Some examples of MOFs that fit this description are ZIF-8, MIL-53, and UiO-66.

Previously, anti-corrosion coatings involved chromate and phosphate-based materials, which posed serious carcinogenic risks.

M. Zhang *et al* studied ZIF-8 and its possibility to act as an anticorrosion film on aluminum plates. ZIF-8 demonstrated excellent anticorrosion characteristics, likely due to its intrinsic hydrophobicity. From this paper, it could be determined that MOFs are strong candidates for future use as anticorrosive films or coatings.<sup>40</sup>

#### 2.8.4 Bifunctional Oxygen Electrocatalysts for Metal Air Batteries

Metal-air rechargeable batteries require a bifunctional electrocatalyst for oxygen reduction and evolution reactions (ORR/OER). Commonly used catalysts for these batteries include Pt, Pd, Ni, Co, and Fe. Pt is very expensive and relatively sparse compared to Pd. The other listed transition metals, while demonstrating strong catalytic activity, were hindered by their relatively low electronic conductivity. To improve these transition metals' conductivity, the catalyst can be doped with electron donors, otherwise known as metal nanoparticles.

Due to their highly porous nature, MOFs are great structures to build these catalysts on. MOFs can be used as a sacrificial template to finely tune the synthesis of these catalysts. In H. Li *et al*, the pyrolysis of MOF ZIF-67 was used to synthesize Pd@PdO-Co<sub>3</sub>O<sub>4</sub> nanocubes to be used as an ORR/OER catalyst. It was determined that this synthesis produced a catalyst with favorable electrocatalytic properties, and a high stability for both oxygen reduction and evolution reactions. With physicochemical characterizations, a layer of CoOOH on the surface of the PdO/Co<sub>3</sub>O<sub>4</sub> prevented further oxidation of the catalyst, as well as provided more active sites for OER reactions.<sup>41</sup>

#### 2.8.5 Natural Gas Storage

Natural gas (NG), which is mainly methane gas is a favorable form of energy compared to other fossil fuels. This is because NG has a high hydrocarbon ratio and a lower carbon dioxide

emission rate compared to fossil fuels. Methane also has a lower energy density, which as limited its ability to be applied on a larger scale in today's world.

Using a sol-gel synthesis (similar to that of aerogels/xerogels), the MOF HKUST-1 was synthesized to experiment with its ability to store methane. This synthesis does not require high pressure or binders to complete. To test the methane absorption rates, volumetric adsorption isotherms of methane were run at room temperature and up to 70 bar.

It was concluded that this MOF could hold and outstanding  $259 \text{ cm}^3 \text{ (STP) cm}^{-3}$  at 65 bar. With such a high affinity to store methane, the practical use of NG in real world applications becomes a much more achievable feat.<sup>42</sup>

## 3.0 Experimental

### 3.1 HPLC Configuration Optimization

In order to optimize the HPLC configuration to ensure that it has the least amount of dead volume possible, RTD steps with through each component were conducted. The HPLC system used was an Agilent 1100 with binary pumps and a 6-port VICI Valco column switching valve for column direction. The detector is an Agilent UV-VIS G1315-60022 diode array detector with a path length of 10 mm and a detection range from 190 nm – 950 nm. The injector system that was used was a G1313A, with a switching valve between the bypass or through the injector needle. The HPLC contains two solvent reservoir bottles, one with water as a carrier and one with Rhodamine RT at 0.1 ppt concentration in water. Injections of 5  $\mu\text{L}$  of Rhodamine RT were introduced to the system flow to identify the concentration and wavelength needed to ensure proper profiles. The concentrations analyzed were: 0 ppm, 0.01 ppm, 0.1 ppm, 1 ppm, 0.001 ppt, 0.1 ppt, and 1 ppt. Beer's Law analysis was then conducted on the peak intensity for each concentration to determine the maximum detectable concentration that would not peg out the detector. Figure 16 shows three points plotted to get a linear fit that can be used to find the molar absorptivity. This value helps to determine the concentration from the HPLC.

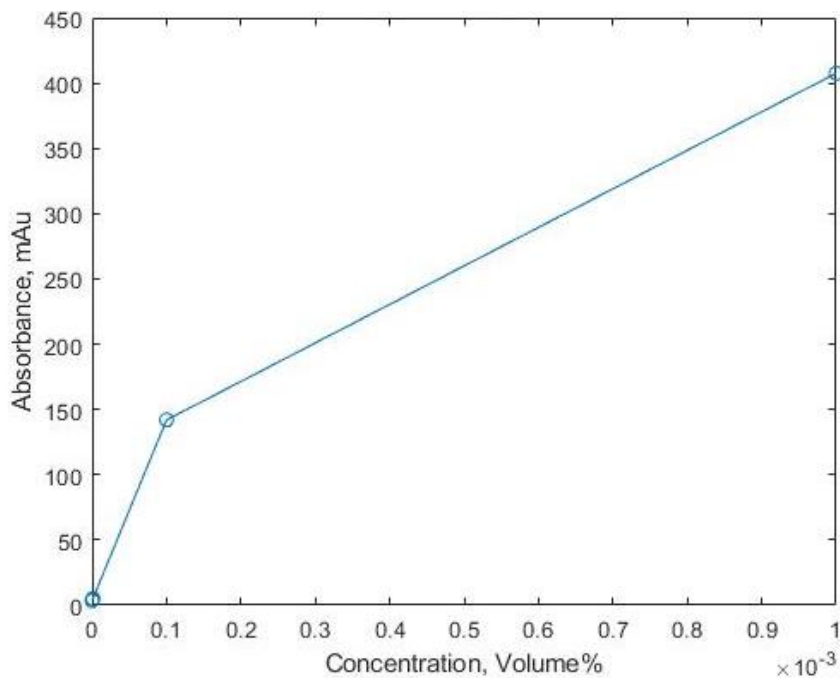


Figure 16: Beer's Law graph of Rhodamine RT at 198nm.

Once the concentrations and wavelength were determined to be 1 ppt and 550 nm respectively, these were then used in each configuration. Figure 16 shows the setup for each individual run.

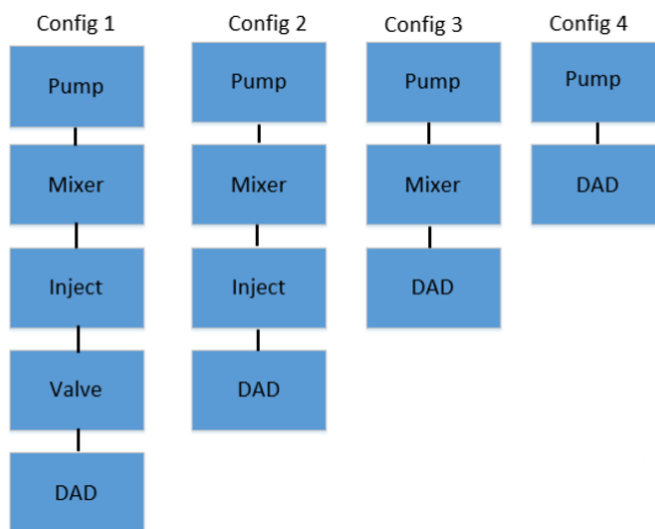


Figure 16: Various HPLC configurations including the indicated components used in each trial

Overall the hope would be to include the most amount of equipment possible to maximize functionality while also having the least amount of dead volume that causes axial dispersion in the flow profiles. Each configuration was screened under six flows and these were all graphed to be set in bar graphs against each other. The flows were 0.5 mL/min to 3.0 mL/min with 0.5 mL intervals. The initial run was 15 minutes of run time with 3.5 mL/min of water and sorbate runs for five minutes. A runoff time of five minutes was then used for each of the flows. Results will be discussed in section 3.8.1.

### 3.2 ZLC System Validation

Ideally the system would be benchmarked against a) published sorbate/sorbent diffusion data in a liquid ZLC system, b) published sorbate/sorbent diffusion data in a non-ZLC system, or c) diffusion of an alternate sorbate/sorbent system (e.g. zeolite). However, due to the lack of research in the testing of liquid-based ZLC systems, this paper surmised the most effective way to validate our system was using the Wilke-Chang relationship to estimate the solute/solvent diffusion coefficient, then correct it for the confined solid pore diffusion. The Wilke-Chang relationship provides a method for estimating the diffusion coefficient of paracetamol in a liquid solvent. This theory applies to nonelectrolytes in an infinitely dilute solution and is described by the equation:

$$D_{AB} = \frac{7.4 * 10^{-8}(\phi_B M_B)^{0.5} T}{V_A^{0.6} \mu_B} \quad (14)$$

Correction factors that depend on a ratio of the solute diameter to the diameter of the pore are used to convert the diffusion coefficient solved by the Wilke-Chang to a diffusion coefficient that describes a hindered solute diffusing through solvent filled pores. This ratio is defined as:

$$\varphi = \frac{d_s}{d_{pore}} \quad (15)$$

The first correction factor is based on geometric arguments for steric exclusion. The equation used to describe this interaction is shown below:

$$F_1(\varphi) = (1 - \varphi)^{0.5} \quad (16)$$

The second correction factor is referred to as the hydrodynamic hindrance factor. This is based on the hindered Brownian motion of a solute particle moving through a solvent filled pore. The equation describing this motion is shown below:

$$F_2(\varphi) = 1 - 2.104\varphi + 2.09\varphi^3 - 0.5\varphi^5 \quad (17)$$

The total correction to the diffusion of a solute in a solvent is described by the equation:

$$D_{Ae} = D_{AB}F_1(\varphi)F_2(\varphi) \quad (18)$$

### 3.3 Paracetamol Extraction

To obtain paracetamol (acetaminophen) to be used in the pharmaceutical trials, twenty 500 mg acetaminophen tablets (CVS brand) were crushed up by mortar and pestle. The resulting powder was then fully dissolved in 200 ml of ethanol. The solution was then filtered through filter paper. Finally, the resulting solution after filtering was heated to evaporate the remaining ethanol. The solid that remained in the glassware after all of the ethanol was evaporated was assumed to be paracetamol, while the binder remained on the filter paper as it does not dissolve in ethanol. 8.14 g of a fluffy white solid was recovered. To characterize the solid powder, XRD analysis was conducted and it could be concluded that the powder was paracetamol.

#### 3.3.1 Paracetamol Characterization

XRD data from the extracted paracetamol can be seen in Figure 17 and Figure 18. According to the MDI Jade software used, the material extracted was in fact paracetamol. MDI Jade concluded with an FOM value of 2.1 (exact match being 0).

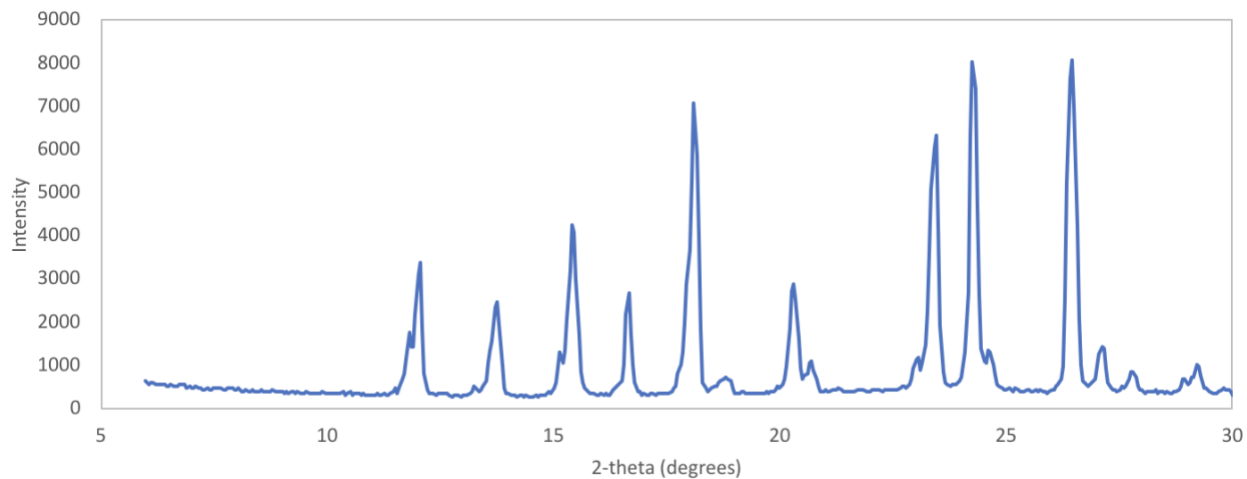


Figure 17: Paracetamol XRD Results

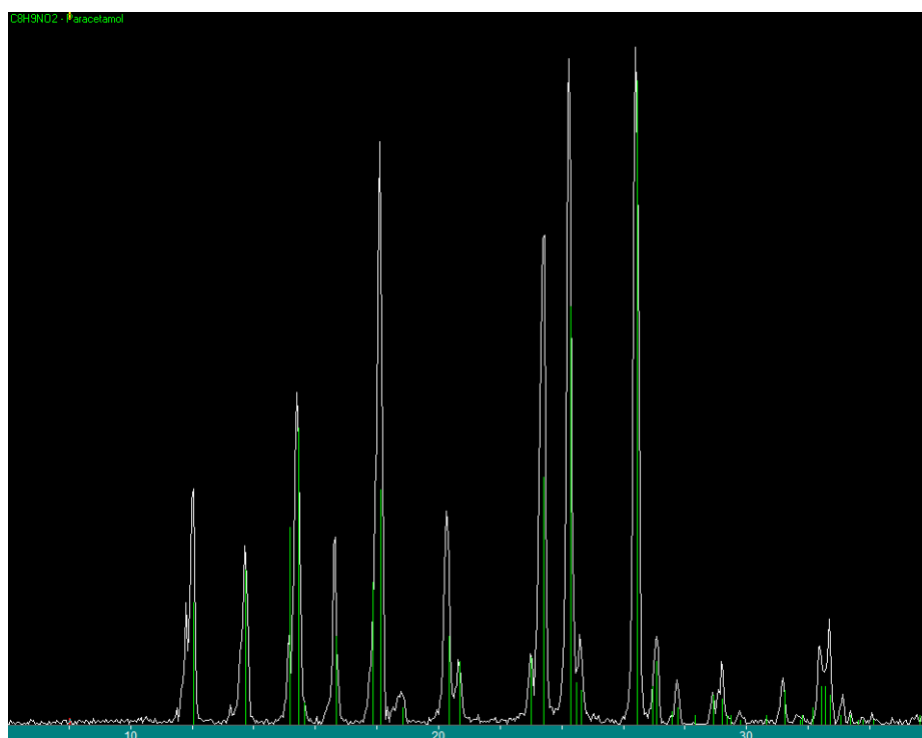


Figure 18: XRD results of paracetamol (white) overlaid with MDI Jade database peaks of paracetamol (green)

The HPLC also provided a way to compare the absorbance spectrum of the paracetamol through a 200 - 310 nm wavelength. The literature value that worked best for our system was found to be at 198 nm. DAD UV data was not included, but it showed agreement with the literature.<sup>43</sup>

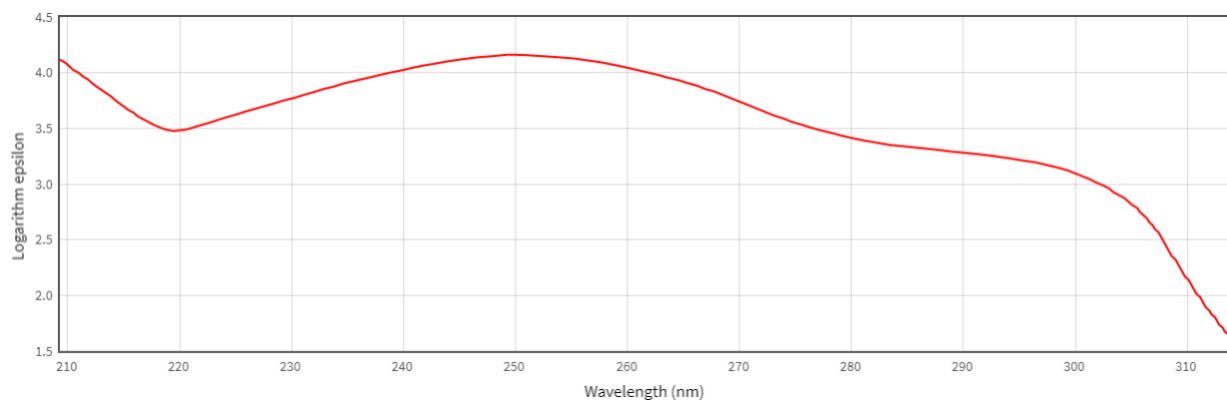


Figure 19: Literature UV data<sup>43</sup>

### 3.4 Zeolite Ion Exchange

The trials for the ZLC system validation were conducted using two different zeolites. They are the Zeolite H-Y and the ion exchanged Zeolite-NaY. The reasoning behind picking these zeolites is due to their large pore openings (0.74 nm), high crystallinity, strong water stability and ready availability on campus. It was obtained from Zeolyst, a commercial zeolite supplier. An ion exchange on the zeolite was conducted to ensure that the numerical model worked across two different structures. In order to perform an ion exchange, 1.0 g of Zeolite Y was mixed into a 1.0 M solution of sodium nitrate for 20 minutes. This solution was then filtered by vacuum filtration to remove the sodium nitrate. This washing was performed three times before drying in the oven for 24 hours at 100°C.<sup>44</sup> To ensure that the product was actually ion exchanged, XRD was conducted on the sample.

Figure 20 showed the graph compared the Zeolite-NaY that was constructed to the baseline in MDI Jade package. The yield in physical material from the washing was 12% based on a mass balance. Lower yields likely arose from the poor seal on the vacuum pump and the use of large pore filter paper that allowed for most of the sample to permeate. While this was not the ideal situation, the axial dispersion in the ZLC meant that small amounts were needed for the trials in the HPLC.

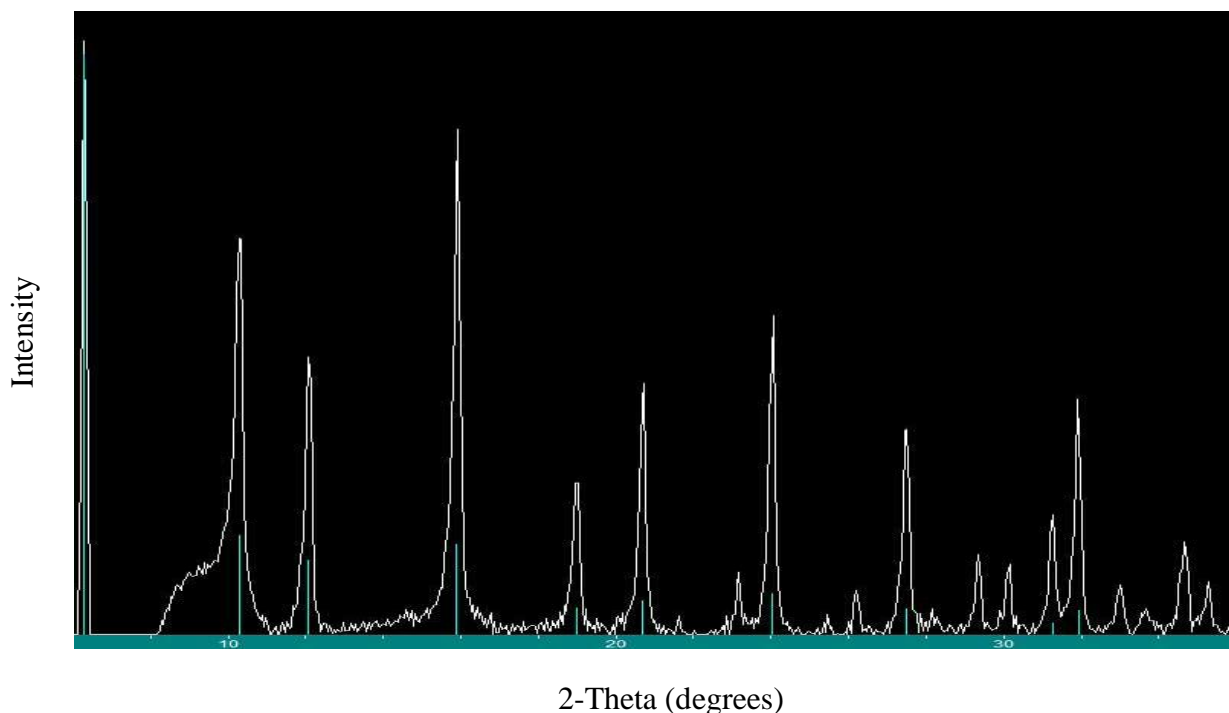


Figure 20: XRD graph of Zeolite NaY (white line) and green markers denoting the location of peaks for a Zeolite NaY from MDI Jade.

The baseline of the XRD shows the structure of a faujasite (FAU) according to the MDI Jade program. The program found that the Zeolite-NaY that was tested was similar with an FOM of 1.8 (exact match being zero) to the Zeolite-NaY in its database. The similarity means that the ion exchange was successful and that it was stable even after drying.

### 3.5 Zeolite Diffusion Trials

After the system was configured to the most realistic dead volume without waste, Beer's Law analysis was conducted on the paracetamol that was previously synthesized. Concentrations of 0.001 g, 0.005 g, 0.01 g, and 0.021 g were used and then 0.0673 g was chosen at a wavelength of 198 nm. The concentration of 0.001 g/1.5 mL was still too high when converting to 1 L, so a magnitude dilution of 10 was don't to bring it to a concentration of 1 ppt that is used throughout all the trials. Trials on the paracetamol were conducted were using the configuration from the first

mixing spot to the detector, or Configuration 1. The first trial involved taking the uptake and release profile of the paracetamol without the ZLC being packed as a background. This run help to normalize the data set through the zero-length column with the zeolite and later the MOF trials. Once the background is taken, 5 mg of the zeolite (Zeolite Y for the first two trials and then Zeolite-NaY for the other three trials) was added and washed with 300 mL of water to remove fine particles that could clog the downstream tubing. The trials for the zeolites were conducted with flows of 0.5 mL/min to 3.0 mL/min with intervals of 0.5 mL/min. Initially three different timescales for the sorbate was used to find determine if the peak absorbance was occurring and that there was a profile that could be found for the steps. There was no difference to be seen in the peaks so a consistent run time of 5 min was used for all trials in the report besides these three. A runoff of 60 minutes for each flowrate. The desorption profiles from these steps are then used to find the residence time of the paracetamol in the zeolite to be entered into the mathematical model that was created.

### 3.6 MOF Synthesis

To synthesize IRMOF-1 for use in the HPLC, the synthesis described in Sabouni, R *et al.*<sup>2</sup> was used. 0.947 g of zinc nitrate hexahydrate and 0.176 g of terephthalic acid (TPA) powders were separately weighed out. Each powder was then transferred into a 25 ml Teflon reactor. 10 ml of diethylformamide (DEF) was added to the teflon reaction vessel. The resulting mixture was mixed well to dissolve the powders into the solvent. Once fully dissolved, the teflon reactor was capped, and inserted into a pressure bomb. The bomb was fully tightened and the capsule was placed in a 100°C oven for 20 hours. After the 20 hour crystallization period, the pressure bomb was removed from the oven and the reaction was quenched by placing the capsule in room temperature water. After quenching the reaction, the contents of the teflon reactor were transferred into a vial to be

used in a centrifuge. The batch was centrifuged at 1500 RPM for 20 minutes. The remaining solvent was decanted from the top. Approximately 15 ml carbon tetrachloride was added to the dried crystals, and the centrifuge process was repeated. Finally, after the crystals were decanted a second time, the contents were placed into a petri dish and left in the oven at 100°C overnight and weighed the following day.

### 3.6.1 MOF Characterization

To characterize the frameworks synthesized, x-ray diffraction and physisorption methods were used. The XRD data can be found below. This curve was compared to literature data. The peaks at 9 and 17 are very prominent, which strongly suggests the presence of IRMOF-1 in the sample. For a more detailed analysis of this characterization and possible degradation, refer to section 4.5.

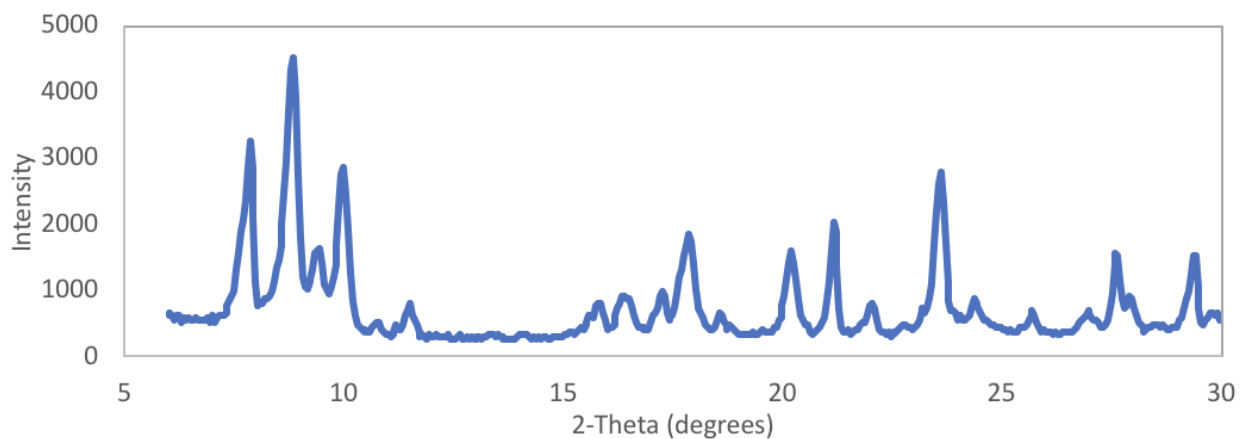


Figure 21: First IRMOF-1 Synthesis

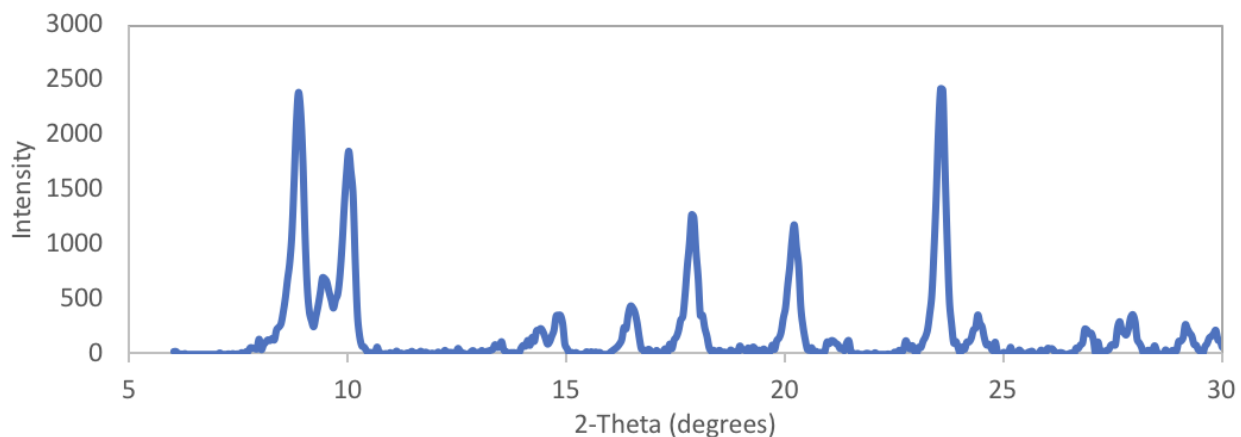


Figure 22: Second IRMOF-1 Synthesis

The physisorption data was acquired from the program Quantachrome® ASiQwin™ through the Autosorb iQ Station. The trial was run with a Nitrogen Adsorbate model using a temperature of 77.35K and a pressure of 33.5 atm. The trial ended prematurely after four points due to the low amount of sample (0.0281 g degassed) that was used. Such a small amount of MOF was used because the synthesis did not provide enough for the 0.05 g that is typically used. The resulting micropore surface area was found through the Dubinin-Radushkevich (DR) equation that is selective for larger pore sizes and uses the region points that were available. The resulting micropore surface area was 82.601 m<sup>2</sup>/g and a micropore volume of 0.0299 cm<sup>3</sup>/g. The literature values for IRMOF-1 was 450 m<sup>2</sup>/g and 0.18 cm<sup>3</sup>/g.<sup>45</sup> The reason for the difference is discussed in section 4.5.

### 3.7 MOF Trials

The amount of MOF loaded into the ZLC was 5mg and this was washed through with 300 mL of water to clear out the fine particles. Trials with the MOF were conducted were using the same method and configuration from the trials with the zeolites in Section 3.5. Figure 23 shows the data from the HPLC as steps. The peaks are when running the sorbate, paracetamol, and the valleys are the washout with water.

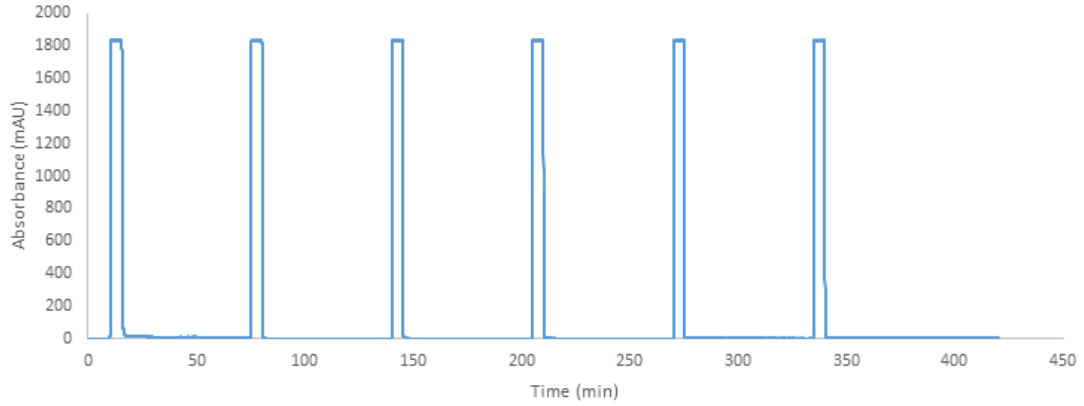


Figure 23: Example of steps from HPLC. This trial is paracetamol at 198nm through IRMOF-1.

### 3.8 Mathematical Model

#### 3.8.1 System Optimization

The main procedure towards optimizing the system involved testing different HPLC configurations and measuring residence time of Rhodamine-WT. Initially, raw data from the HPLC was collected (Figure 24) and normalized using Equation (17).

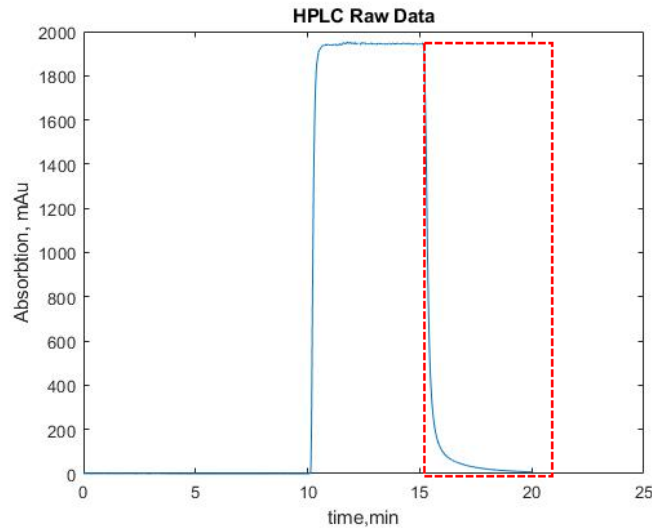


Figure 24: HPLC raw data with red box indicating desorption profile

$$\text{Dimensionless Concentration} = \frac{y - y_{min}}{y_{max} - y_{min}} = \frac{C}{C_o} \quad (19)$$

Y is the absorbance at any point in time,  $Y_{\min}$  is the minimum absorbance value (baseline value), and  $Y_{\max}$  is the maximum absorbance value corresponding to the initial concentration in the liquid. All “Y” values in Equation (19) are taken from the desorption region of the HPLC data, which is outlined with a dashed red line in Figure 24. After the concentration was normalized it was fit to an exponential decay using Equation (20). This exponential fit data was then plotted vs time, shown in Figure 25 below.

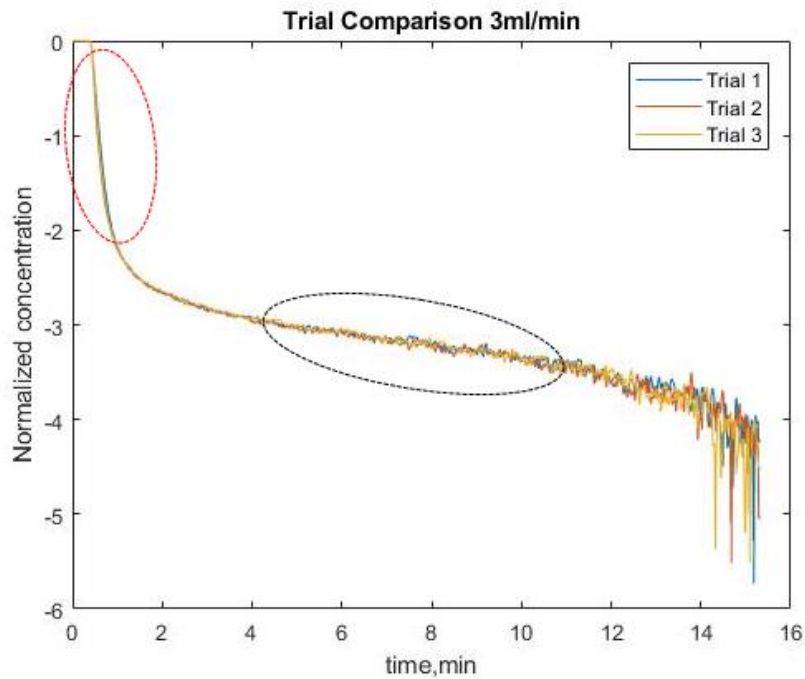


Figure 25: Normalized Concentration on Log-Scale vs. Time

The region circled in red is the short time region, or the washout region. The slope of this region is equal the negative value of the residence time, so multiplying the slope by negative one gives the residence time. This slope was found by using the polyfit function in Matlab for a first order polynomial. Once the residence time is found, it is converted from minutes to seconds and plotted against the inverse of the flow rate it. According to Equation (20) the plot of the inverse flow rate vs residence time should have a slope equal to the dead volume of the system.

$$V_D = \tau * F \quad (20)$$

In Equation (20),  $V_D$  is the dead volume,  $\tau$  is the residence time, and  $F$  is the flow rate of the liquid phase. An example of this plot can be seen in Figure 26, which shows the same configuration tested 3 times to show that results are repeatable.

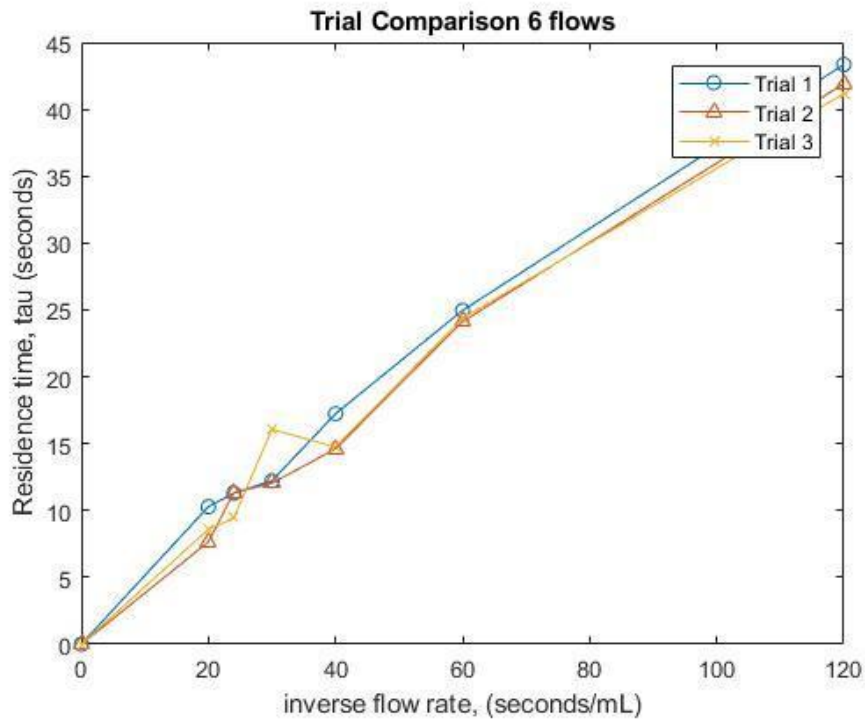


Figure 26: Residence Time ( $\tau$ ) vs. Inverse Flowrate showing a linear relationship in accordance with equation (20)

This full procedure to find dead volume was done in Matlab for different configurations at various flow rates. Once each configuration is tested and dead volume calculated, they were plotted on a bar graph so that the differences for each configuration could be seen clearly.

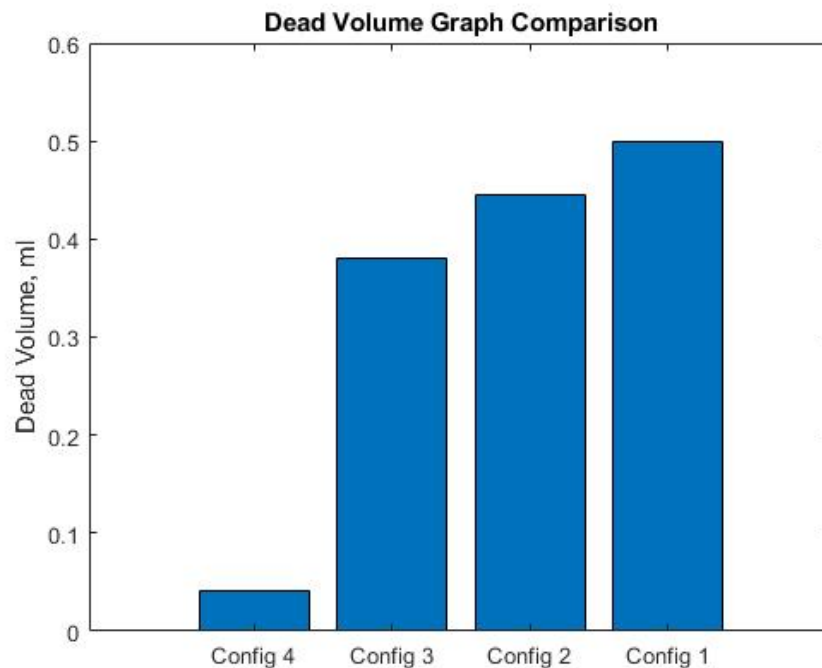


Figure 27: Comparison of Dead Volume for Different Configurations

The 0.5 mL of dead volume is significantly larger than the overall volume of the sorbent. There is only 0.001 mL of MOF/zeolite as 5 mg were added at a density of 0.5 g/cm<sup>3</sup>. Configuration 4 was chosen to best minimize the overall dead volume to ensure that long desorption profiles were not needed to beat the washout time. Configuration 4 was not as efficient with the sorbent in the ZLC, possibly due to increased turbidity in the column due to the particles presence. When the zeolite was washed out of the ZLC, it was found to affect the dead volume in the system. Further trials with Zeolite Y and Zeolite-NaY saw the dead volume rise initially and then decrease with Configuration 4 to 1.5 mL for Zeolite-Y and 0.45 mL for Zeolite-NaY. This is likely due to dispersion in the ZLC chamber as a result of particles blocking the flow path. These are the values that are used in the results when running the Matlab script to fit the ZLC model to the data.

### 3.8.2 Diffusivity Modeling

Diffusivity modeling was carried out in Matlab by numerically solving the solid phase mass balance (Equation (8)). A Matlab script was created to solve Equation (8) as a boundary value problem using Equations (9) and (10) as initial conditions and the first boundary condition at the center of the particle, respectively. The final boundary condition for concentration at surface of the particle must be solved for simultaneously with the overall mass balance by an estimated diffusion coefficient. The overall goal is to create a model that reproduces the profiles in Figure 25 as accurately as possible, with emphasis on accurately modeling the slope of the long-time region which is circled in black. The final script numerically solves Equation (8) and will accurately approximate data from the ZLC at different flow rates when provided with a proper estimation for  $D_{AB}$ .

The concentrations were normalized and plotted versus time. The main procedure to solve Equation (8) as a boundary value problem in Matlab was to use the `bvp4c` function. This function evaluates the solid phase mass balance using appropriate boundary conditions and initial conditions. The variables  $q$  and  $r$  were represented in Matlab by  $y$  and  $x$ .

The boundary condition at the center of the particle was set so that the change in concentration at the center of the particle was zero due to symmetry. At the surface, the boundary condition defines the concentration as a function of the particle radius, particle volume, diffusivity, system dead volume, mobile phase flow rate, and Henry's constant between the mobile phase and particle surface. This boundary condition is defined below:

$$C_s = \frac{-V_f * L}{F * R^2} * \frac{dq}{dt} - \frac{L}{R^2} * y_1 \quad (21)$$

In Equation (21),  $V_f$  is dead volume,  $F$  is mobile phase flow rate,  $R$  is particle radius,  $y$  is the concentration of the sorbate, and  $L$  is a variable related to flow rate, particle radius, particle volume, Henry's constant, and diffusivity. The variable  $L$  is defined below in Equation (22).

$$L = \frac{1}{3} * \frac{F * R^2}{K * V_s * D_{AB}} \quad (22)$$

Where  $V_s$  is the volume of the particle and  $K$  is the Henry Constant. Since the concentration being calculated is normalized, the initial concentration was set to  $q=1$  at  $t=0$ .

Since the `bvp4c` function can only solve for one solution at a time, Equation (8) is only evaluated after a single “time step”.

In order to get a solution over the full period of time, a for loop was created to evaluate the equation between  $t=0$  and the final time,  $t_f$ . All values for concentration, or  $y$ , are defined in a vector of a length the time vector plus one. The value of  $y_1$  and  $y_0$  are defined as the value of  $y$  at column “ $i$ ” and “ $i-1$ ” in the theta vector, respectively. This allows for the mass balance to be evaluated with the proper concentrations over the full length of time.

Having properly input the equation into Matlab, the resulting concentration were plotted versus time. The diffusivity  $D_{AB}$  is changed (tuned) until the desorption profiles match those obtained from the ZLC. Therefore, the value of  $D_{AB}$  that gave the proper profile is the diffusion coefficient of our material. A copy of the code can be found in [Appendix B: Matlab Code](#).

In addition to the Matlab model, a simplified analytical solution to the math model was also used for rapid verification of our system. This version assumes that there is no fluid-phase hold-up which reduces the equations<sup>22</sup>:

$$\frac{c(t)}{c_o} = \sum \frac{2L}{\beta_n^2 + (1 - L + \gamma\beta_n^2)^2 + L - 1 + \gamma\beta_n^2} x \exp(-\beta_n^2 \frac{D}{R^2} t) \quad (23)$$

$$\beta_n \cot\beta_n + L - 1 - \gamma\beta_n^2 = 0 \quad (24)$$

Where Equation (23) is the desorption curve model and Equation (24) is down to the form of:

$$\frac{c}{c_o} = 2L \sum \frac{\exp[-\beta_n^2 \left(\frac{D}{R^2}\right) t]}{\beta_n^2 + L(L-1)} \quad (25)$$

$$\beta_n \cot \beta_n + L - 1 = 0 \quad (26)$$

This assumption allows for ease of calculation of diffusion coefficient. However, values calculated from this model are only meant to be used as a reference for the full model since this is an oversimplification of the system.<sup>22</sup>

### 3.9 Safety

Proper safety precautions in regards to typical lab protective equipment was utilized. Nitrile gloves were sufficient for the chemicals used while thermal gloves were used for removing samples from the oven. The zeolite was ion exchanged and loaded into the ZLC in the presence of a fume hood due to its ability to irritate lungs and eyes. The ion exchange utilized a sodium nitrate base that was properly diluted to safe pH to be disposed of in the sink. When setting up the pressure chamber for the MOF drying, it was filled to less than half way to ensure that the solvent evaporation did not cause an explosion due to pressurization. Links to the SDS pages for sodium nitrate, terephthalic acid, Zeolite Y, zinc nitrate hexahydrate, and diethylformamide can be found in Appendix C: SDS Sheets.

## 4.0 Results and Discussion

### 4.1 Particle Size and Volume Distribution

Images of our suspension of particles were taken with one sample shown in Figure 29 using an optical microscope. These images were analyzed using the Particle Analysis Method in the ImageJ software to obtain particle size and volume distributions as shown in Figure 30 and Figure 31. The montage shown in Figure 28 below shows the process by which these particles were analyzed.

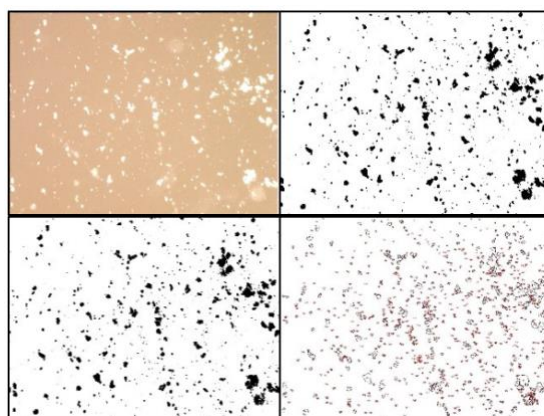


Figure 28: Montage of Steps for Particle Analysis Method

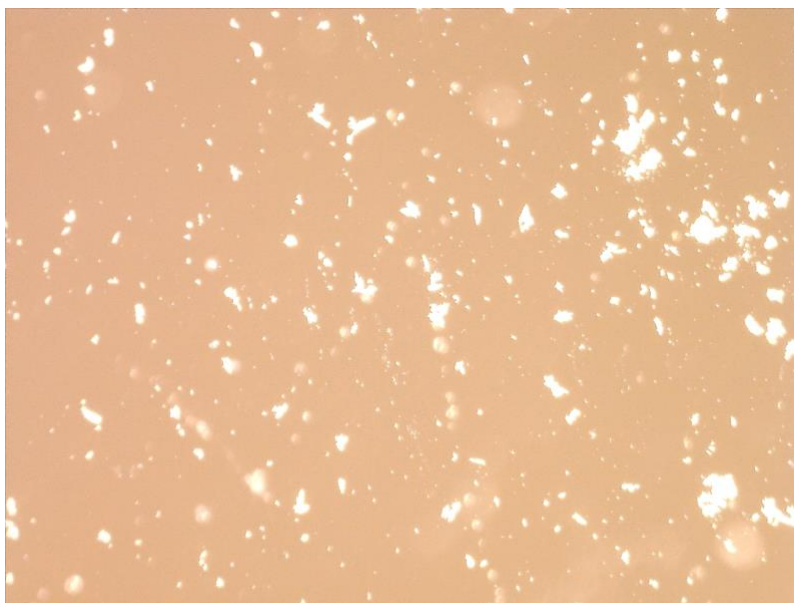


Figure 29: Optical Image of MOF-5 Particles

The mean particle size was shown to be  $\sim 6 \mu\text{m}$  and approximately 1600 particles having a volume equal to or less than  $500 \mu\text{m}^3$ . However, there were 500 particles recorded to have volumes equal to or greater than  $10,000 \mu\text{m}^3$ . This may be due to agglomerates not being completely watershed during the analysis process, thus they were deemed artifacts and were omitted from further analysis.

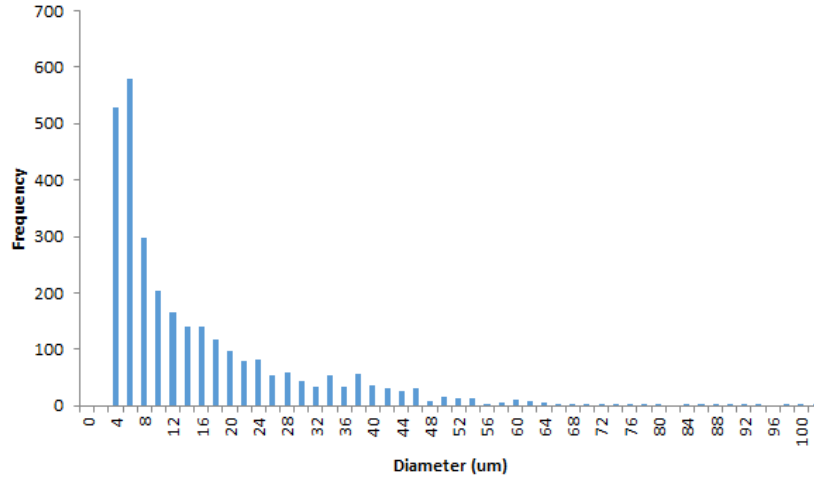


Figure 30: Particle Diameter Distribution Using Data from ImageJ

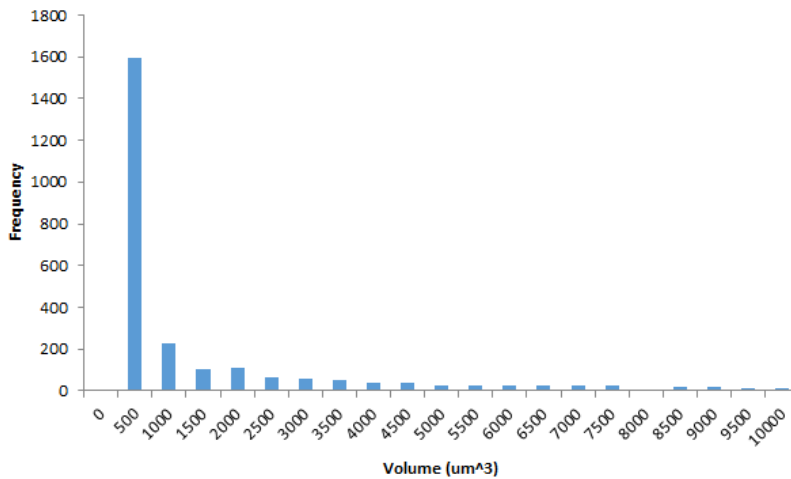


Figure 31: Particle Volume Distribution Using Data from ImageJ

## 4.2 Analysis of Methods Used for Modelling

The raw data from desorption curves of the HPLC with no species in the ZLC were run through two different programs to understand the differences and the selectivity of a numerical solution versus an approximate analytical solution. The approximate analytical solution was run through an excel file that fit the parameters of a gas phase mobile phase was the case in Brandini and Ruthven. The numerical solution was solved using a boundary value problem and partial differential equation script in Matlab to model the short and longtime profile of the desorption curve. With the Matlab script, the raw data was converted to dimensionless concentration and plotted on a log scale vs time. In order to understand the background to the data that was being collected, the first trial that was run through the two analyses was the baseline. The baseline graph of paracetamol through a ZLC with just the two frits inside can be seen in Figure 32 (A). The baseline as shown in the figure shows that the model approximates an empty cell when the diffusion coefficient would be approaching infinity.

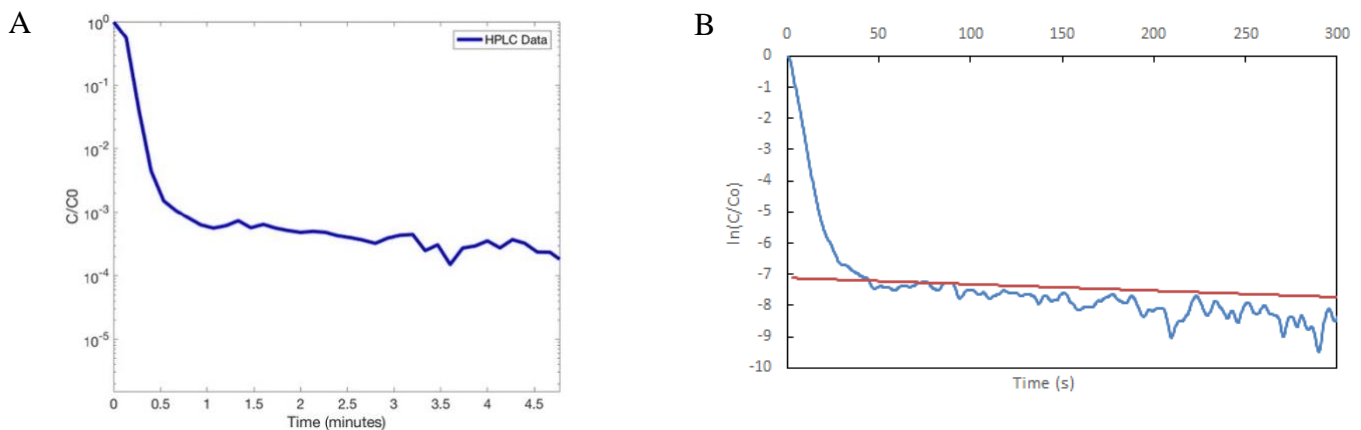


Figure 32: (A) Normalized desorption profile through an empty ZLC chamber.  $F = 0.5$  ml/min  
(B) Baseline of ZLC run in Excel (blue) and fit (red),  $F = 0.5$  ml/min

Figure 32 shows the washout dominated over a diffusion coefficient. No diffusion model was able to accurately describe the desorption profile. The closest fit (shown in Figure 32 (B)) resulted in a diffusion coefficient of  $3.78 \times 10^{-14} \frac{m^2}{s}$  using the excel gas phase method. The Matlab version was unable to fit the long-time region as the washout occurred too rapidly.

### 4.3 Diffusion Measurements in Zeolite System Validation

#### 4.3.1 Approximate Analytical Model Fitting

Zeolite-Y and Zeolite-NaY were both tested to show that the system works before IRMOF-5 was used. As shown in Figure 33, Zeolite-Y is substantially different from the control data (blank cell). This data shows close agreement with the fit line as the time range chosen for fit was 400-800 seconds since this is where the long-time occurs for these data sets. Both fits produced diffusion coefficients within 3% of each other and the values produced show that Zeolite-Y is not affected by the presence of water as the average diffusion coefficient calculated was  $2.82 \times 10^{-16} m^2/s$ . This is two orders of magnitude smaller than that of the measured baseline which means that there is holdup in the zeolite structure that is removed after washout.

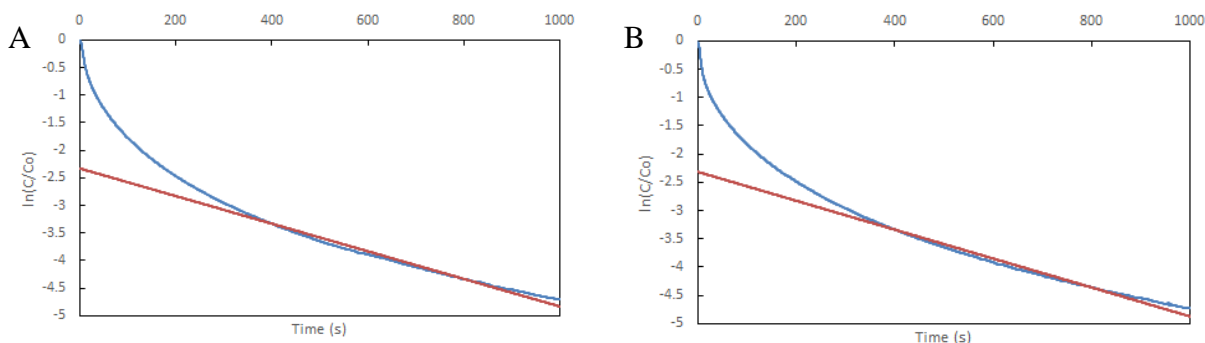


Figure 33: (A) Zeolite-Y Trial 1,  $F = 0.5 \text{ ml/min}$ , (B) Zeolite-Y Trial 2,  $F = 0.5 \text{ ml/min}$

Zeolite-NaY was tested within the column using three different uptake times (one minute, five minute, and one hour) to ensure that the proper peak was reached before desorption began. The three did not have an appreciable difference and the standard 5 min runs that were used in all

trials was chosen. Figure 35 shows dimensionless concentration profiles of the different uptake times fit to the same model. The model fit well to the experimental data and produced similar diffusion coefficients as shown in Table 2. The change in the start of the long-time diffusion may be because there was not as much paracetamol allowed to saturate the Zeolite-NaY so the washout time was quick.

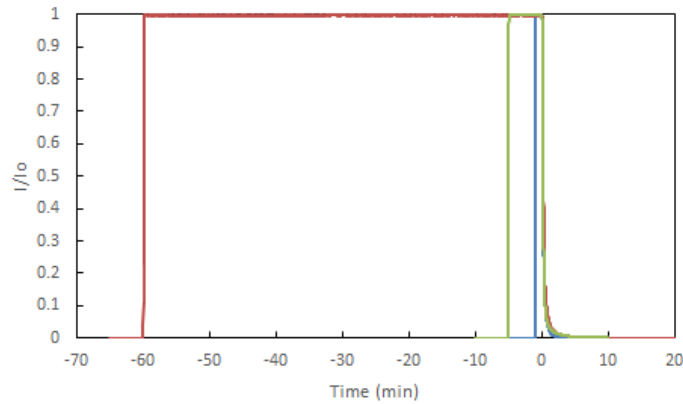


Figure 34: Normalized Raw Data for One Hour Uptake (red), Five Minute Uptake (light green), and One Minute Uptake (blue)

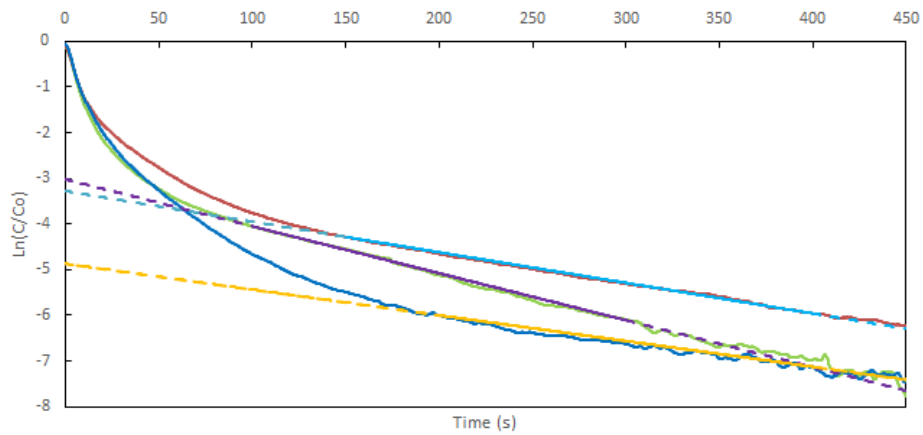


Figure 35: Comparison of Zeolite-NaY Uptake Times; Five Minute (light green), Five Minute Fit Line (purple), One Hour (red), One Hour Fit Line (light blue), One Minute (dark blue), and One Minute Fit Line (yellow)

Table 2: Uptake time comparison based on Diffusion Coefficient of Zeolite-Y

<b>Trial</b>	<b>Diffusion Coefficient (m<sup>2</sup>/s)</b>
Zeolite-NaY One Minute	5.76 x 10 <sup>-16</sup>
Zeolite-NaY Five Minute	1.09 x 10 <sup>-15</sup>
Zeolite-NaY One Hour	8.31 x 10 <sup>-16</sup>

Each trial was run with a five-minute uptake and thus, comparatively, Zeolite-Y showed a lower diffusion coefficient than that of Zeolite-NaY as shown in Table 3. This may be occurring because in the ion exchange, hydrogen ions are being replaced by sodium ions. In addition to this, the zeolite is also becoming partially dealuminated meaning that the structure is now becoming more porous and thus will allow the paracetamol to diffuse more rapidly into and out of the ion-exchanged zeolite. Lee and Rees performed the same ion-exchange, instead using HCl as the acid, and 56% of the framework aluminum was released.<sup>46</sup>

Table 3: Diffusion coefficient comparison between Zeolite-Y and Zeolite-NaY

<b>Trial</b>	<b>Diffusion Coefficient (m<sup>2</sup>/s)</b>
Zeolite-Y 5 Minute Trial 1	2.79 x 10 <sup>-16</sup>
Zeolite-Y 5 Minute Trial 2	2.85 x 10 <sup>-16</sup>
Zeolite-NaY 5 Minute Trial 1	1.09 x 10 <sup>-15</sup>

#### 4.3.2 Numerical Solution Fits of Zeolite Runs

The numerical analysis with Matlab showed the same trends as the gas phase model found but it ultimately found diffusion coefficients that were significantly lower than previously thought. Figure 36 show the profiles for the trials.

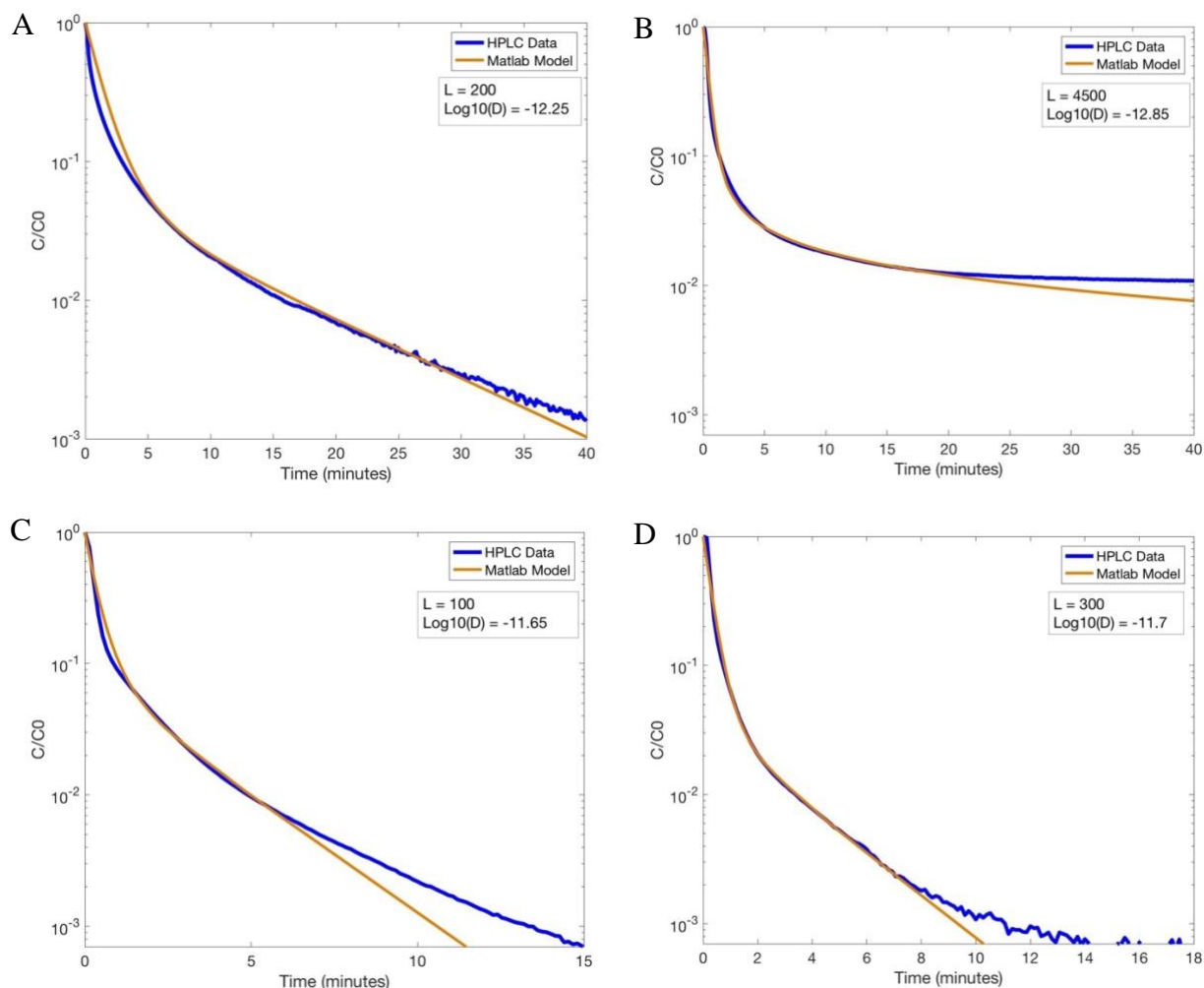


Figure 36: (A) Zeolite Y trial 1,  $F = 0.5$  ml/min, strong agreement is observed at both short and long times, (B) Zeolite NaY trial 1,  $F = 0.5$  ml/min, (C) Zeolite NaY One Minute Uptake,  $F = 0.5$  ml/min, (D) Zeolite NaY One Hour Uptake,  $F = 0.5$  ml/min, note time scales

Table 4 and Table 5 have the values for each trial in a way that makes them easy to compare. They all are slower than the baseline diffusion which means that washout did not dominate the whole ZLC. An interesting result was that the five minute uptake of paracetamol in Zeolite-NaY produced the slowest diffusion coefficient out of all the trials. It is possible that it was an outlier or there could be more going on there. The scale of the diffusion is consistent with literature values of a liquid phase with solid molecules going through zeolites. Literature shows that diffusion of molecules through a porous media of approximately 2 nm is around  $10^{-12}$  m<sup>2</sup>/s.<sup>47,48</sup>

Table 4: Uptake time comparison based on Diffusion Coefficient of Zeolite-Y

<b>Trial</b>	<b>Diffusion Coefficient (m<sup>2</sup>/s)</b>
Zeolite-NaY One Minute	2.24 x 10 <sup>-12</sup>
Zeolite-NaY Five Minute	1.4 x 10 <sup>-13</sup>
Zeolite-NaY One Hour	2 x 10 <sup>-12</sup>

Table 5: Diffusion coefficient comparison between Zeolite-Y and Zeolite-NaY

<b>Trial</b>	<b>Diffusion Coefficient (m<sup>2</sup>/s)</b>
Zeolite-Y 5 Minute Trial 1	5.6 x 10 <sup>-13</sup>
Zeolite-NaY 5 Minute Trial 1	1.4 x 10 <sup>-13</sup>

## 4.4 IRMOF Results

### 4.4.1 IRMOF Diffusion Coefficient Model

Raw data of the adsorption of paracetamol onto the surface of IRMOF-1 was converted to dimensionless concentration. The simplified model was used to predict the diffusion coefficient of IRMOF-1. Figure 37 show fits to the IRMOF-1 data and these fits do not agree well with the long-time data as well within the 50-200 second time range fitted. This is a result of the degradation of the diffusivity properties of IRMOF-1. This occurs because when water interacts with IRMOF-1, water blocks active sites on the surface of the MOF and does not desorb and thus the MOF is not able to work properly.<sup>51</sup> Humidity in the process of construction of the MOF can lead to improper synthesis and lead to washout of MOF components in the liquid system. Figure 37 (D) shows the MOF data run through the Matlab script. The diffusion coefficient being ten to the negative eight means that washout is dominant in the ZLC and that the IRMOF is not having any uptake of the paracetamol and is rather just a product of a change in dead volume.

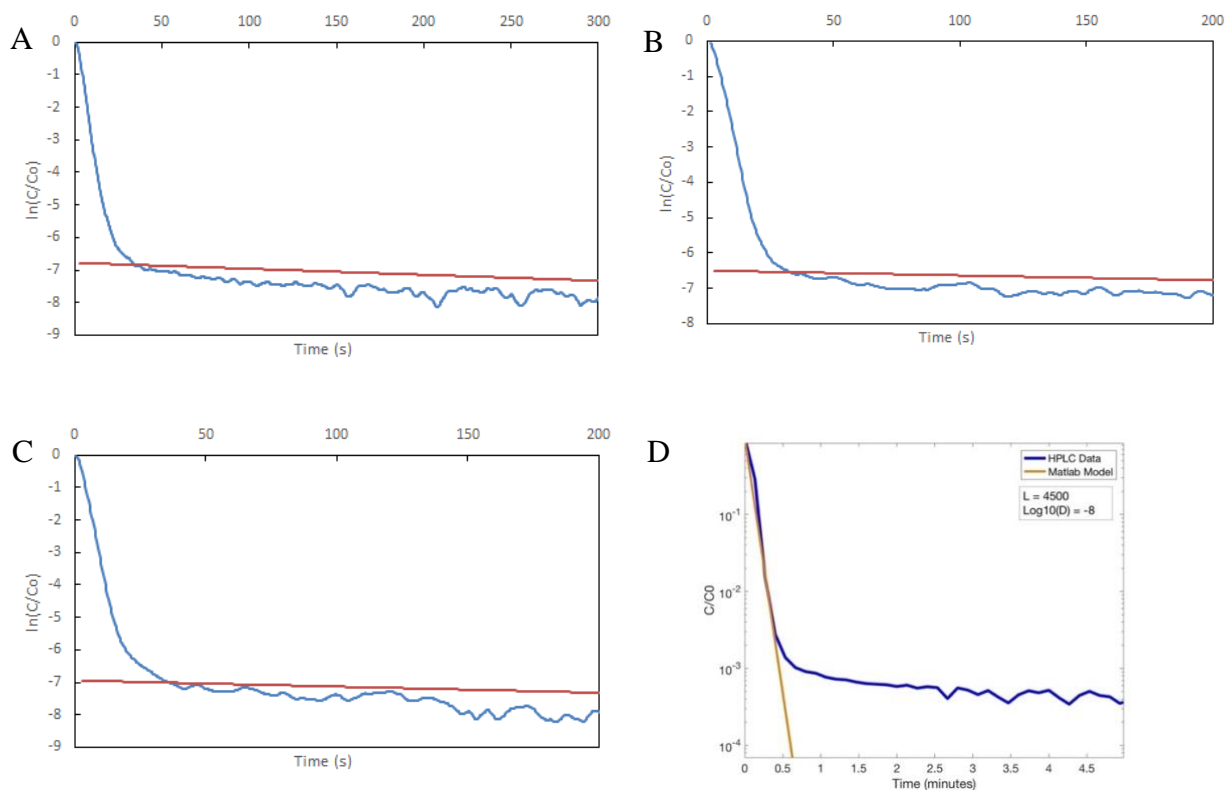


Figure 37: (A) Data Fit with IRMOF-1; dimensionless concentration (blue) and fit curve (red),  $F = 0.5$  ml/min, (B) Data Fit with IRMOF-1; dimensionless concentration (blue) and fit curve (red),  $F = 0.5$  ml/min, (C) Data Fit with IRMOF-1; dimensionless concentration (blue) and fit curve (red),  $F = 0.5$  ml/min, (D) Matlab Model for MOF Diffusivity showing the short-time desorption profile model. Long time diffusion is indistinguishable from background detector noise,  $F = 0.5$  ml/min

This phenomenon is more obvious when using our model to estimate the diffusion coefficients for three sets of MOF data and a blank data set. As shown in

Table 6, the diffusion coefficients show great agreement with each other which is expected because if the active sites on IRMOF-1 are not available for paracetamol to adsorb onto then the solution will just flow around it and so it will show a diffusion coefficient to that of the blank run. See section 4.5 for more detail. Another observation that makes sense is that the diffusion coefficients of the MOF trials is slightly less than that of the blank run. This is because even though the paracetamol is not able to adsorb to the MOF, the presence of the MOF presents a hindrance

to flow and thus diffusion coefficient should be slightly lower than that of the blank run. Washout dominates the system and there is only a slight deviation in dead volume which leads to the change in what is found to be a diffusion coefficient.

Table 6: IRMOF-1 and Blank Diffusion Coefficient Values

<b>Trial</b>	<b>Diffusion Coefficient (m<sup>2</sup>/s)*</b>
Blank	3.78 x 10 <sup>-14</sup>
IRMOF-1 Trial 1	2.49 x 10 <sup>-14</sup>
IRMOF-1 Trial 2	1.91 x 10 <sup>-14</sup>
IRMOF-1 Trial 3	2.65 x 10 <sup>-14</sup>

\*These values were model fits that do not physically represent the intraparticle diffusion coefficient

Lastly, all of the compounds were overlaid and compared in Figure 38. It is shown that the IRMOF-1 data and the Blank run show similar profiles and overlap which is expected since the IRMOF-1 active sites for adsorption are being blocked by water molecules. Zeolite-Y and Zeolite-NaY, however, show much slower desorption profiles representing that paracetamol is able adsorb to the surface and desorb accordingly. These zeolites show the ability for controlled drug release by modifying Zeolite-Y used for drug storage. Slower release profiles can thus be achieved by continuing to modify the Zeolite-Y or Zeolite-NaY structures.

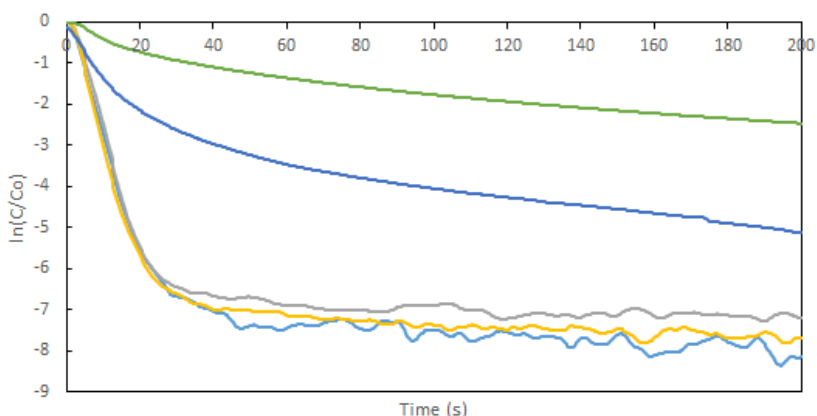


Figure 38: Comparison of Blank (light blue), IRMOF-1 Trial 1 (yellow), IRMOF-1 Trial 2 (gray), IRMOF-1 Trial 3 (orange), Zeolite-NaY (blue), and Zeolite-Y (light green)

#### 4.4.2 IRMOF-1 Results Compared to Model

The IRMOF-1 data was compared to more than one model used for estimating the diffusion coefficient. One such model used was the Wilke-Chang relationship. This model looks at hindered solute diffusion through tiny capillary holes. As shown in Table 7, the Wilke-Chang relationship predicts a diffusion coefficient that is three orders of magnitude faster than that of the average measured IRMOF-1. One reason for this may be that the Wilke-Chang relationship assumes an infinitely dilute solution which can mean that the solute molecules are only interacting with the solvent molecules and not other solute molecules. This means that the model is not accounting for additional interactions that the acetaminophen is experiencing. This assumption does not hold up since the concentration of the acetaminophen used for running trials was one part per thousand which is far beyond the assumption of infinitely dilute. Another reason this model may not be accurately predicting the diffusion coefficient is that the molal volume had to be estimated using Table 24.5 from *Fundamentals of Momentum, Heat, and Mass Transfer* (Welty).<sup>5</sup> The molal volume is proportional to the diffusion coefficient by the  $-0.6$  power so it can play an important role in the final diffusion coefficient value. It may also be possible that the correction factors may under predict the diffusion coefficient as it does not account for how tortuous the path of diffusion is.

Table 7: Comparing Wilke-Chang Relationship to Experimental Data

	<b>Diffusion Coefficient (m<sup>2</sup>/s)</b>
<b>Wilke-Chang</b>	1.42 x 10 <sup>-11</sup>
<b>Avg. IRMOF-1</b>	2.35 x 10 <sup>-14</sup>

## 4.5 Impurities in MOF

Upon analysis of the XRD characterization of the MOF, it could be determined that the crystals were in the presence of the unreacted terephthalic acid and zinc nitrate hexahydrate from the synthesis. As can be seen in the figures below, there are peaks that match between the MOF XRD pattern and the XRD patterns of the precursors.

There are a few possible explanations for this contamination. (1) The duration of the crystallization period followed from Sabouni, R *et al* (2010)<sup>2</sup> was not long enough, which left some of the precursors unreacted, (2) the cleaning process post-synthesis was not sufficient, or (3) the crystal structure of the MOF was compromised due to humidity in the environment.

As can be seen in Figure 39, a peak at 23 seems to correlate between the synthesized IRMOF-1 samples, as well as zinc nitrate hexahydrate from Figure 40.

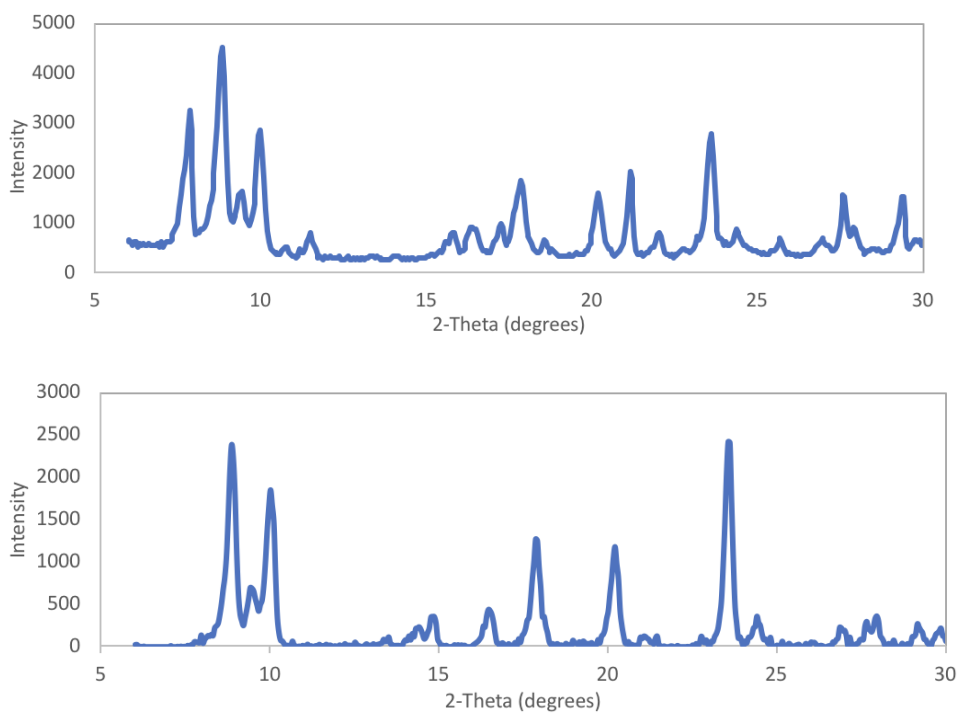


Figure 39: XRD results from first (top) and second (bottom) MOF syntheses

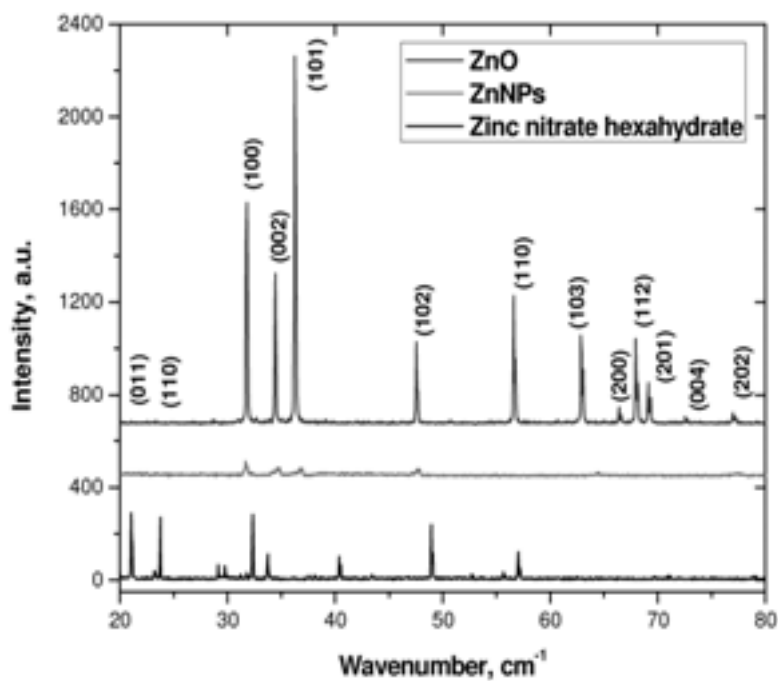


Figure 40: XRD Pattern of Zinc Nitrate Hexahydrate<sup>49</sup>

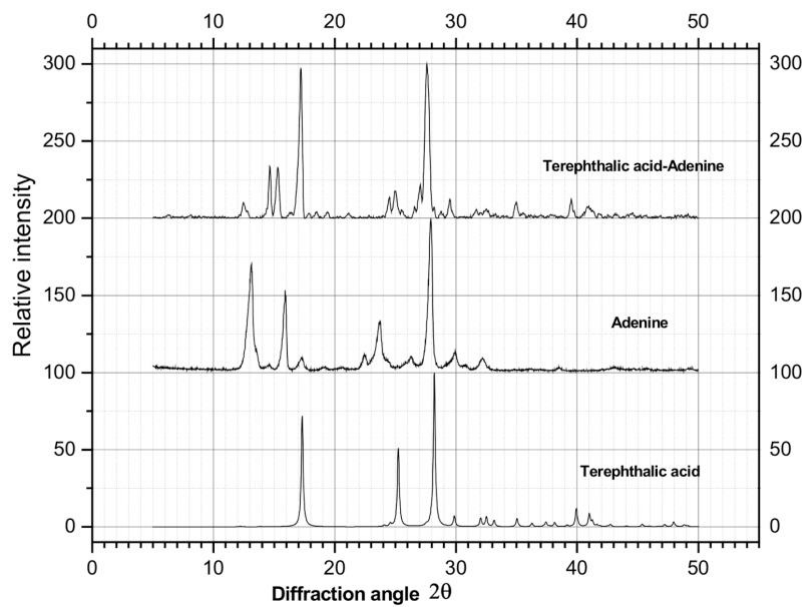


Figure 41: XRD Pattern of Terephthalic Acid<sup>50</sup>

To prevent leftover precursor from remaining in the powdered MOF, this research suggests that the cleaning process post-synthesis should be improved. The centrifugation step of the cleaning process should be repeated at least 5 times to ensure that any unreacted precursor.

According to Ming *et al*, MOF-5's properties are limited due to absorption of water due to humidity in the air. This could cause the crystal structure to swell and deform, which could cause unexpected peaks, or shift the peaks' locations in the XRD data.<sup>51</sup> Figure 42 overlays the XRD data obtained from the IRMOF-1 synthesis to the data collected by Ming *et al*. The peaks at 2-theta values of 9 and 17 strongly correlate with each other. This suggests that the IRMOF-1 crystal structure degraded in the presence of water before XRD data could be collected.<sup>51</sup>

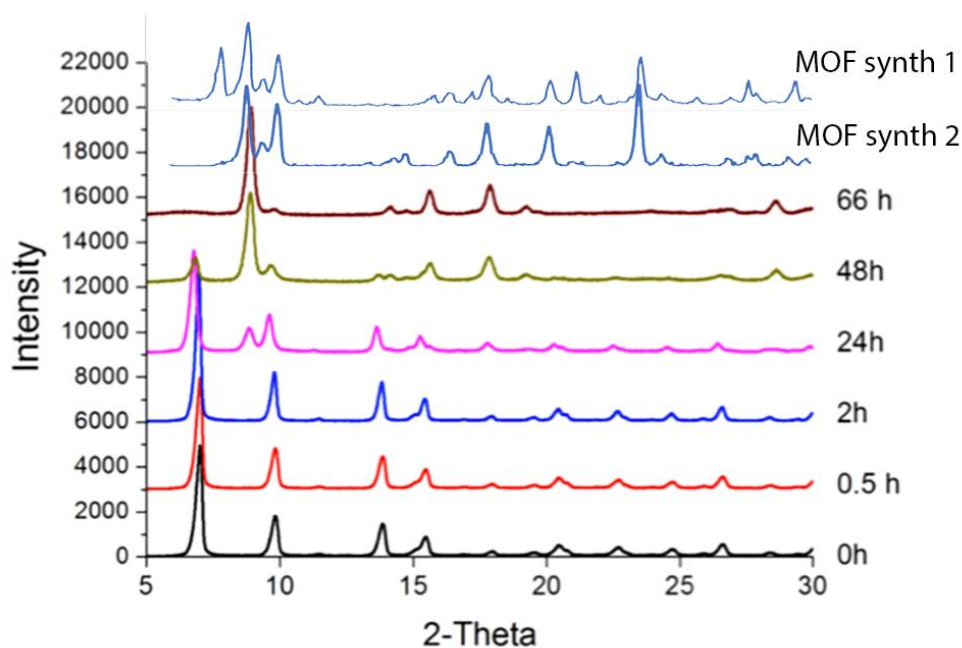


Figure 42: XRD of MOF-5 at multiple time steps in the presence of a 61% humidity environment<sup>51</sup>

To alleviate this issue of degradation, Asiabi *et al*. has modified MOF-5 with a methyl group, which has proven to prevent the degradation of the framework when in the presence of water to a degree.<sup>52</sup>

## 5.0 Conclusion

### 5.1 Main Findings

The main findings of this MQP regard the successful modeling of desorption profiles in a ZLC model using Zeolites-Y and Zeolite-NaY, the synthesis and characterization of IRMOF-1, and the degradation of the structure of IRMOF-1 in water. Due to the data from the HPLC from the trial with a blank column and with IRMOF-1 being nearly identical, it can be concluded that IRMOF-1 degrades in water making it a poor candidate for drug delivery. The mass balance around the ZLC proposed by Brandani & Ruthven was solved numerically, yielding desorption profiles that accurately predict HPLC data in both the short time (washout) and longtime regions.

### 5.2 Future Work

For future work, it is recommended to use a more water stable MOF, such as HKUNST-1, or MOFs with different pore sizes for diffusive property studies. Furthermore, it is recommended that different APIs (i.e. cancer treatment drugs) are studied that have different particle sizes as the desorption profiles will change with different sorbents and MOF structures. Additionally, using a solvent and temperature that mimics the environment in the human body would be more accurate for drug delivery studies.

Direct work that could be done to further the work made in this project would be to vary the amount of MOF or Zeolite into the system. This project assumed axial dispersion in the ZLC because diffusion is typically obtainable through common projections of diffusion through a few molecules. While this is typically true, it is something that would bolster the argument and ensure that nothing happens with a variance in amounts. Finally, determining the effects that higher flow rates have on the diffusion of the API in the MOF or zeolite would also be important, as our study showed the effects but the ultimate scope of the project didn't include indexing the flow rates, but rather focused on obtaining a model for both the zeolite and the MOF individually.

## 6.0 References

---

- <sup>1</sup> Boehle, T. File:IRMOF-1 wiki.png [https://commons.wikimedia.org/wiki/File:IRMOF-1\\_wiki.png](https://commons.wikimedia.org/wiki/File:IRMOF-1_wiki.png) (accessed Mar 16, 2018).
- <sup>2</sup> Sabouni, R.; Kazemian, H.; Rohani, S. A novel combined manufacturing technique for rapid production of IRMOF-1 using ultrasound and microwave energies. *Chemical Engineering Journal* **2010**, *165*(3), 966–973.
- <sup>3</sup> Horcajada, P.; Chalati, T.; Serre, C.; Gillet, B.; Sebrie, C.; Baati, T.; Eubank, J. F.; Heurtaux, D.; Clayette, P.; Kreuz, C.; Chang, J.-S.; Hwang, Y. K.; Marsaud, V.; Bories, P.-N.; Cynober, L.; Gil, S.; Férey, G.; Couvreur, P.; Gref, R. Porous metal–organic-Framework nanoscale carriers as a potential platform for drug delivery and imaging. *Nature Materials* **2009**, *9*(2), 172–178.
- <sup>4</sup> Rashid Usman, M. Transport Phenomena-Mass Transfer, 2016
- <sup>5</sup> Welty, J. R. *Fundamentals of Momentum, Heat, and Mass Transfer*; Wiley: New York, 2015.
- <sup>6</sup> Kim, C.-ju. *Advanced Pharmaceuticals: Physiochemical Principles*; CRC Press: Boca Raton (Fla.), 2004.
- <sup>7</sup> Davis, M. E.; % Davis, R. J. *Fundamentals of Chemical Reaction Engineering*; *Dover Publications*, New York, 2012
- <sup>8</sup> Fogler, H. S. *Elements of Chemical Reaction Engineering*, 4<sup>th</sup> ed.; *Prentice Hall*, Upper Saddle River, 2006
- <sup>9</sup> Wittrup, K. D. *Course materials for 10.37 Chemical and Biological Reaction Engineering*, Spring, *MIT*. 2007
- <sup>10</sup> Crowther, J.; Dowling, J.; Hartwick, R.; & Ciccone, B. Performance qualification of HPLC instrumentation in regulated laboratories. *LCGC North America*. 2008
- <sup>11</sup> Teuscher, N. What is HPLC/UV? *Certara*. 2014.
- <sup>12</sup> Hong, V. & Wrolsted, R. E. Use of HPLC separation/photodiode array detection for characterization of anthocyanins. *J. Agric. Food Chem.* 1990
- <sup>13</sup> Fornstedt, T.; Forssen, P.; & Westerlund, D. *Analytical Separation Science*. Wiley-VCH Verlag GmbH & Co. KGaA. 2015
- <sup>14</sup> Malenovic, A.; Ivanovic, D.; Medenica, M.; Jancic, B.; & Markovic, S. Retention modelling in liquid chromatographic separation of simvastatin and six impurities using a microemulsion as eluent. *J. of Separation Science*. 2004

- 
- <sup>15</sup> Biomolecules <http://chemistry.tutorvista.com/analytical-chemistry/biomolecules.html> (accessed Mar 16, 2018).
- <sup>16</sup> Torres, J. To run or to fly: A comparison between HPLC and GC. *BitesizeBio*
- <sup>17</sup> Supap, T.; Idem, R.; Tontiwachwuthikul, P.; & Saiwan, C. Analysis of monoethanolamine and its oxidative degradation produced during CO<sub>2</sub> absorption from flue gases: A comparative study of GC-MS, HPLC-RID, and CE-DAD analytic techniques and possible optimum combinations. I&EC Research. 2006
- <sup>18</sup> HITACHI. Principle and feature of various detection methods. 2018
- <sup>19</sup> Dolan, J. W. How Does It Work? Part IV: Ultraviolet Detectors <http://www.chromatographyonline.com/how-does-it-work-part-iv-ultraviolet-detectors> (accessed Mar 7, 2018).
- <sup>20</sup> Brandani, S. ZLC Basics, 2007
- <sup>21</sup> Ruthven, D. M.; Stapleton, P. Measurement of liquid phase counter-Diffusion in zeolite crystals by the ZLC method. *Chemical Engineering Science* **1992**, 48(1), 89–98.
- <sup>22</sup> Brandani, S.; Ruthven, D. M. Analysis of ZLC Desorption Curves for Liquid Systems. *Chemical Engineering Science* **1995**, 50(13), 2055–2059.
- <sup>23</sup> Koohsaryan, E.; Anbia, M. Nanosized and hierarchical zeolites: A short review. *Chinese Journal of Catalysis* **2016**, 37(4), 447–467.
- <sup>24</sup> Yates, D. J. C. Studies on the surface area of zeolites, as determined by physical adsorption and X-Ray crystallography. *Canadian Journal of Chemistry* **1968**, 46(10), 1695–1701.
- <sup>25</sup> B. Jha; D.N. Singh, Fly Ash Zeolites; Springer Singapore, 2016; p 5
- <sup>26</sup> Cho, Y.; Lee, J.-Y.; Bokare, A. D.; Kwon, S.-B.; Park, D.-S.; Jung, W.-S.; Choi, J.-S.; Yang, Y.-M.; Lee, J.-Y.; Choi, W. LiOH-Embedded zeolite for carbon dioxide capture under ambient conditions. *Journal of Industrial and Engineering Chemistry* **2015**, 22, 350–356.
- <sup>27</sup> Weitkamp, J. Catalysis and Zeolites. *Solid State Ionics* **1999**, 175–188.
- <sup>28</sup> Inglezakis, V. J. The concept of “capacity” in zeolite ion-Exchange systems. *Journal of Colloid and Interface Science* **2005**, 281(1), 68–79.
- <sup>29</sup> B. Jha; D.N. Singh, Fly Ash Zeolites; Springer Singapore, 2016; p 9
- <sup>30</sup> Kalogeras, I.; Vassilikou-Dova, A. Electrical Properties of Zeolitic Catalysts. *Defect and Diffusion Forum* **1998**, 164, 1–36.

- 
- <sup>31</sup> Furukawa, H.; Cordova, K. E.; Okeeffe, M.; Yaghi, O. M. The Chemistry and Applications of Metal-Organic Frameworks. *Science* **2013**, *341*(6149), 1230444–1230444.
- <sup>32</sup> Eddaoudi, M.; Moler, D. B.; Li, H.; Chen, B.; Reineke, T. M.; Okeeffe, M.; Yaghi, O. M. Modular Chemistry: Secondary Building Units as a Basis for the Design of Highly Porous and Robust Metal–Organic Carboxylate Frameworks. *Accounts of Chemical Research* **2001**, *34*(4), 319–330.
- <sup>33</sup> Metal Organic Frameworks with Ultrahigh Porosity for Carbon Capture <http://www.cchem.berkeley.edu/molsim/teaching/fall2011/CCS/Group7/background.htm> (accessed Mar 7, 2018).
- <sup>34</sup> Krishna, R.; Baten, J. M. V. A comparison of the CO<sub>2</sub> capture characteristics of zeolites and metal–organic frameworks. *Separation and Purification Technology* **2012**, *87*, 120–126.
- <sup>35</sup> Vaughan, O. Porous by design. *Nature* **2014**.
- <sup>36</sup> Cai, W.; Chu, C.-C.; Liu, G.; Wang, Y.-X. J. Metal-Organic Framework-Based Nanomedicine Platforms for Drug Delivery and Molecular Imaging. *Small* **2015**, *11*(37), 4806–4822.
- <sup>37</sup> Ferey, G.; C. Mellot-Draznieks, C.; Serre, C.; Millange, F.; Dutour, J.; Surlblé, S.; Margiolaki, I. A Chromium Terephthalate-Based Solid with Unusually Large Pore Volumes and Surface Area. *Science* **2005**, *309*(5743), 2040–2042.
- <sup>38</sup> Sun, C.-Y.; Qin, C.; Wang, C.-G.; Su, Z.-M.; Wang, S.; Wang, X.-L.; Yang, G.-S.; Shao, K.-Z.; Lan, Y.-Q.; Wang, E.-B. Chiral Nanoporous Metal-Organic Frameworks with High Porosity as Materials for Drug Delivery. *Advanced Materials* **2011**, *23*(47), 5629–5632.
- <sup>39</sup> Rojas, S.; Carmona, F. J.; Maldonado, C. R.; Horcajada, P.; Hidalgo, T.; Serre, C.; Navarro, J. A. R.; Barea, E. Nanoscaled Zinc Pyrazolate Metal–Organic Frameworks as Drug-Delivery Systems. *Inorganic Chemistry* **2016**, *55*(5), 2650–2663.
- <sup>40</sup> Zhang, M.; Ma, L.; Wang, L.; Sun, Y.; Liu, Y. Insights into the Use of Metal–Organic Framework As High-Performance Anticorrosion Coatings. *ACS Applied Materials & Interfaces* **2018**, *10*(3), 2259–2263.
- <sup>41</sup> Li, H.-C.; Zhang, Y.-J.; Hu, X.; Liu, W.-J.; Chen, J.-J.; Yu, H.-Q. Metal-Organic Framework Templated Pd@PdO-Co<sub>3</sub>O<sub>4</sub> Nanocubes as an Efficient Bifunctional Oxygen Electrocatalyst. *Advanced Energy Materials* **2018**, 1702734.
- <sup>42</sup> Tian, T.; Zeng, Z.; Vulpe, D.; Casco, M. E.; Divitini, G.; Midgley, P. A.; Silvestre-Albero, J.; Tan, J.-C.; Moghadam, P. Z.; Fairen-Jimenez, D. A sol–gel monolithic metal–organic framework with enhanced methane uptake. *Nature Materials* **2017**, *17*(2), 174–179.
- <sup>43</sup> Talrose, V.; Yermakov, A. N.; Usov, A. A.; Goncharova, A. A.; Leskin, A. N.; Messineva, N. A.; Trusova, N. V.; Efimkina, M. V. Acetaminophen. *NIST Chemistry WebBook*. 2018

- 
- <sup>44</sup> Danaher, P. J.; Medino, C.; Shevchuk, H.; & Zhang, E. M. *Testing the stability of cation exchanged zeolite ZSM-5 in hot liquid water*. Worcester Polytechnic Institute. 2017
- <sup>45</sup> Ozkan, U. S. *Design of Heterogeneous Catalysis*. John Wiley & Sons. Hoboken, 2009
- <sup>46</sup> Beyer, H. K. *Dealumination Techniques for Zeolites*, Springer-Verlag: Berlin Heidelberg, 2002.
- <sup>47</sup> Zeolyst International. <http://www.zeolyst.com/our-products/standard-zeolite-powders/zeolite-y.html> (Accessed March 21, 2018)
- <sup>48</sup> Schuring, D. *Diffusion in Zeolites: Towards a Microscopic Understanding*. Ph.D. Dissertation, Technical University of Eindhoven, The Netherlands, 2002.
- <sup>49</sup> Rao, C.; Golder, A.; Bhakal, K. BIOMEDIATED SYNTHESIS OF ZNO NANOPARTICLES (ZNONPS) FOR PHOTOCATALYTIC APPLICATION. *INTERNATIONAL JOURNAL OF CURRENT ENGINEERING AND SCIENTIFIC RESEARCH* **2014**, 26–30.
- <sup>50</sup> Perumalla, S. R.; Suresh, E.; Pedireddi, V. R. Nucleobases in Molecular Recognition: Molecular Adducts of Adenine and Cytosine with COOH Functional Groups. *Angewandte Chemie* **2005**, 117(47), 7930–7935.
- <sup>51</sup> Ming, Y.; Kumar, N.; Siegel, D. J. Water Adsorption and Insertion in MOF-5. *ACS Omega* **2017**, 2(8), 4921–4928.
- <sup>52</sup> Asiabi, M.; Mehdinia, A.; Jabbari, A. Preparation of water stable methyl-Modified metal-organic framework-5/Polyacrylonitrile composite nanofibers via electrospinning and their application for solid-Phase extraction of two estrogenic drugs in urine samples. *Journal of Chromatography A* **2015**, 1426, 24–32.

## Appendix A: Raw Data

Na 1 hour steps

Absorbance	Time
1836.8	310.03
204.05	310.7
68.15	311.36
33.93	312.03
21.68	312.7
15.28	313.36
10.64	314.03
7.29	314.7
4.84	315.36
3.26	316.03
1.46	316.7
0.48	317.36
-0.37	318.03
-0.74	318.7
-1.33	319.36
-1.7	320.03
-1.66	320.7
-2	321.36
-1.92	322.03
-2.11	322.7
-2.19	323.36
-2.29	324.03
-2.48	324.7
-2.4	325.36
-2.37	326.03
-2.44	326.7
-2.51	327.36
-2.61	328.03
-2.6	328.7
-2.67	329.36
-2.51	330.03
-2.56	330.7
-2.73	331.36
-2.73	332.03
-2.81	332.7
-2.58	333.36
-2.71	334.03
-2.77	334.7
-2.74	335.36
-2.88	336.03

Na 1 min steps

Absorbance	Time
1829.36	194.05
119.29	194.71
30.01	195.38
9.89	196.05
4.08	196.71
1.56	197.38
0.32	198.05
-0.37	198.71
-0.78	199.38
-1.3	200.05
-1.67	200.71
-1.82	201.38
-2.1	202.05
-2.41	202.71
-2.59	203.38
-2.76	204.05
-3.01	204.71
-2.98	205.38
-2.93	206.05
-3.15	206.71
-3.1	207.38
-3.24	208.05
-3.03	208.71
-3.36	209.38
-3.35	210.05
-3.36	210.71
-3.09	211.38
-3.29	212.05
-3.31	212.71
-3.14	213.38
-3.3	214.05
-3.4	214.71
-3.44	215.38
-3.3	216.05
-3.35	216.71
-3.21	217.38
-3.35	218.05
-3.1	218.71
-3.21	219.38
-3.42	220.05

-2.9	336.7	-2.86	220.71
Na 1 hour steps		Na 1 min steps	
Absorbance	Time	Absorbance	Time
-3.06	337.36	-3.06	221.38
-2.86	338.03	-2.91	222.05
-2.71	338.7	-2.94	222.71
-2.9	339.36	-2.81	223.38
-2.83	340.03	-2.84	224.05
-2.89	340.7	-2.84	224.71
-2.9	341.36	-2.79	225.38
-2.87	342.03	-3.09	226.05
-3.09	342.7	-2.92	226.71
-2.92	343.36	-2.94	227.38
-3.23	344.03	-2.95	228.05
-3.18	344.7	-2.88	228.71
-3	345.36	-2.91	229.38
-3.15	346.03	-2.78	230.05
-3	346.7	-2.82	230.71
-2.87	347.36	-2.98	231.38
-3.15	348.03	-2.92	232.05
-3.27	348.7	-2.86	232.71
-3.21	349.36	-2.95	233.38
-3.04	350.03	-2.87	234.05
-3.19	350.7	-2.9	234.71
-3.08	351.36	-2.88	235.38
-3.25	352.03	-2.98	236.05
-3.33	352.7	-2.87	236.71
-3.3	353.36	-2.85	237.38
-3.24	354.03	-2.66	238.05
-3.06	354.7	-2.94	238.71
-3.19	355.36	-2.71	239.38
-3.11	356.03	-2.8	240.05
-3.11	356.7	-2.88	240.71
-2.81	357.36	-2.77	241.38
-3.1	358.03	-2.77	242.05
-3.01	358.7	-2.87	242.71
-3.23	359.36	-3.02	243.38
-3.18	360.03	-2.86	244.05
-3.24	360.7	-2.78	244.71
-3.14	361.36	-2.87	245.38
-3.19	362.03	-2.9	246.05
-3.24	362.7	-2.86	246.71
-3.16	363.36	-2.75	247.38
-3.41	364.03	-2.92	248.05

Na 1 hour steps	
Absorbance	Time
-3.14	364.7
-3.22	365.36
-3.12	366.03
-3.42	366.7
-3.19	367.36
-3.04	368.03
-3.4	368.7

Na 1 min steps	
Absorbance	Time
-2.85	248.71
-2.85	249.38
-2.86	250.05
-2.94	250.71
-2.8	251.38
-2.89	252.05
-2.79	252.71

Na March

11

Absorbance	Time
1830.4	210.05
124.28	210.72
49.68	211.39
31.18	212.05
22.43	212.72
15.58	213.39
11.24	214.05
8.79	214.72
6.91	215.39
5.94	216.05
5.41	216.72
4.71	217.39
4.48	218.05
4.31	218.72
3.78	219.39
3.85	220.05
3.75	220.72
3.64	221.39
3.8	222.05
3.43	222.72
3.64	223.39
3.19	224.05
3.47	224.72
3.47	225.39
3.39	226.05
3.52	226.72
3.48	227.39
3.41	228.05
3.05	228.72

Without MOF

Absorbance	Time
2121.85	274.95
-5.92	275.62
-6.61	276.28
-7.15	276.95
-7.4	277.62
-7.64	278.28
-7.42	278.95
-7.67	279.62
-7.57	280.28
-7.64	280.95
-7.96	281.62
-7.68	282.28
-7.64	282.95
-7.82	283.62
-7.82	284.28
-7.67	284.95
-7.66	285.62
-7.5	286.28
-7.69	286.95
-7.6	287.62
-7.66	288.28
-7.81	288.95
-7.69	289.62
-7.75	290.28
-7.7	290.95
-7.77	291.62
-7.73	292.28
-7.62	292.95
-7.78	293.62

Na March 11		Without MOF	
Absorbance	Time	Absorbance	Time
3.38	229.39	-7.76	294.28
3.41	230.05	-7.68	294.95
3.6	230.72	-7.86	295.62
3.76	231.39	-7.53	296.28
3.65	232.05	-7.92	296.95
3.47	232.72	-7.61	297.62
3.76	233.39	-7.5	298.28
3.58	234.05	-8.04	298.95
3.55	234.72	-7.64	299.62
3.57	235.39	-8.03	300.28
3.55	236.05	-7.87	300.95
3.64	236.72	-7.78	301.62
3.65	237.39	-7.86	302.28
3.73	238.05	-8.15	302.95
3.77	238.72	-7.97	303.62
3.64	239.39	-7.99	304.28
3.81	240.05	-7.72	304.95
3.75	240.72	-8.08	305.62
3.65	241.39	-7.87	306.28
3.78	242.05	-8.11	306.95
3.79	242.72	-8.07	307.62
3.83	243.39	-7.86	308.28
3.74	244.05	-7.97	308.95
3.47	244.72	-7.9	309.62
3.67	245.39	-7.73	310.28
3.71	246.05	-8.13	310.95
3.83	246.72	-8.05	311.62
3.76	247.39	-7.94	312.28
3.61	248.05	-8.14	312.95
4.06	248.72	-7.9	313.62
3.93	249.39	-7.87	314.28
3.73	250.05	-7.82	314.95
3.93	250.72	-7.99	315.62
3.76	251.39	-8.03	316.28
3.79	252.05	-8.26	316.95
3.89	252.72	-8.21	317.62
3.51	253.39	-7.7	318.28
3.31	254.05	-7.97	318.95
3.79	254.72	-8.09	319.62
3.92	255.39	-7.92	320.28
3.82	256.05	-8.24	320.95

Na March 11	
Absorbance	Time
3.85	256.72
3.94	257.39
3.9	258.05
3.9	258.72
3.91	259.39
4.02	260.05
3.87	260.72
3.85	261.39
3.93	262.05
3.65	262.72
3.93	263.39
3.98	264.05
4.02	264.72
3.99	265.39
3.92	266.05
3.93	266.72
3.55	267.39
3.98	268.05
3.69	268.72

Without MOF	
Absorbance	Time
-8.09	321.62
-8.07	322.28
-7.97	322.95
-8.13	323.62
-8.03	324.28
-8.14	324.95
-8.24	325.62
-8.25	326.28
-8.16	326.95
-8.12	327.62
-7.89	328.28
-8.15	328.95
-8.16	329.62
-8.19	330.28
-8.47	330.95
-8.31	331.62
-8.1	332.28
-8.15	332.95
-8.1	333.62

With MOF 2-21	
Absorbance	Time
2125.87	274.98
-5.82	275.65
-6.49	276.32
-6.77	276.98
-7.14	277.65
-7.11	278.32
-6.9	278.98
-7.06	279.65
-7.17	280.32
-7.23	280.98
-7.14	281.65
-7.04	282.32
-6.97	282.98
-7.15	283.65
-7.25	284.32
-7	284.98
-7.15	285.65

Zeolite Y	
Absorbance	Time
1754.36	275.04
579.73	275.71
331.84	276.38
217.3	277.04
150.15	277.71
107.03	278.38
77.5	279.04
55.66	279.71
39.35	280.38
26.69	281.04
16.7	281.71
8.69	282.38
2.17	283.04
-3.5	283.71
-7.82	284.38
-11.32	285.04
-14.24	285.71

-7.23 286.32                      -17.47 286.38

With MOF 2-21		Zeolite Y	
Absorbance	Time	Absorbance	Time
-7.06	286.98	-20.05	287.04
-6.99	287.65	-22.56	287.71
-7.07	288.32	-24.59	288.38
-7.15	288.98	-26.26	289.04
-7.09	289.65	-28.2	289.71
-7.2	290.32	-29.46	290.38
-7.1	290.98	-30.97	291.04
-7.11	291.65	-31.97	291.71
-7.1	292.32	-32.59	292.38
-7.14	292.98	-33.43	293.04
-7.3	293.65	-34.38	293.71
-7.16	294.32	-35.21	294.38
-7.04	294.98	-36.07	295.04
-7.12	295.65	-36.58	295.71
-7.22	296.32	-37.6	296.38
-7.48	296.98	-38.27	297.04
-7.04	297.65	-38.64	297.71
-7.18	298.32	-39.23	298.38
-7.27	298.98	-39.85	299.04
-7.34	299.65	-39.9	299.71
-7.26	300.32	-40.81	300.38
-7.09	300.98	-41.09	301.04
-7.28	301.65	-41.49	301.71
-7.29	302.32	-42.04	302.38
-7.23	302.98	-42.16	303.04
-7.42	303.65	-42.58	303.71
-7.66	304.32	-42.81	304.38
-7.41	304.98	-43.18	305.04
-7.42	305.65	-43.44	305.71
-7.58	306.32	-43.37	306.38
-7.32	306.98	-43.77	307.04
-7.29	307.65	-44.08	307.71
-7.11	308.32	-44.22	308.38
-7.3	308.98	-44.4	309.04
-7.55	309.65	-44.62	309.71

-7.31	310.32	-45.07	310.38
-7.37	310.98	-44.92	311.04
-7.36	311.65	-45.22	311.71
-7.45	312.32	-45.3	312.38
-7.77	312.98	-45.46	313.04
-7.51	313.65	-45.52	313.71

With MOF 2-21		Zeolite Y	
Absorbance	Time	Absorbance	Time
-7.55	314.32	-45.84	314.38
-7.38	314.98	-45.85	315.04
-7.41	315.65	-45.78	315.71
-7.38	316.32	-46.24	316.38
-7.58	316.98	-46.34	317.04
-7.47	317.65	-46.47	317.71
-7.44	318.32	-46.51	318.38
-7.51	318.98	-46.38	319.04
-7.19	319.65	-46.66	319.71
-7.56	320.32	-46.7	320.38
-7.48	320.98	-46.83	321.04
-7.68	321.65	-47.12	321.71
-7.55	322.32	-47.04	322.38
-7.59	322.98	-47.32	323.04
-7.46	323.65	-47.42	323.71
-7.56	324.32	-47.34	324.38
-7.62	324.98	-47.37	325.04
-7.79	325.65	-47.53	325.71
-7.57	326.32	-47.45	326.38
-7.67	326.98	-47.53	327.04
-7.85	327.65	-47.53	327.71
-7.64	328.32	-47.72	328.38
-8	328.98	-48.07	329.04
-7.66	329.65	-47.81	329.71
-7.59	330.32	-47.98	330.38
-7.64	330.98	-47.76	331.04
-7.52	331.65	-47.97	331.71
-7.51	332.32	-48.26	332.38
-7.49	332.98	-48.1	333.04

-7.6 333.65

-48.24 333.71

## Appendix B: Matlab Code

### Script 1: Residence times and dead volume for system validation

This script takes raw data from the HPLC and solves for the dead volume of the system. This is done by first grabbing the HPLC data points from the desorption region and normalizing the concentration. The normalized concentration is plotted vs time and the slope of the initial short time region is found by modeling it as a first order polynomial with polyfit. This slope is used to find the washout time and the washout time is plotted as a function of the inverse of the flow rate that the data was collected at. The slope of the washout time vs inverse flow rate graph is the dead volume of the configuration.

```
clc
clear

%Converting HPLC Data from excel file into a string
str=["Data 1.xlsx","Data 2.xlsx","Data 3.xlsx"];

%Importing Absorbance data from the previously defined string for
%each flow rate, q
for i=1:3

    Data=xlsread(str(i));
    q05(1:9101,i)= Data(10500:19600,2);
    q1(1:9101,i)=Data(28500:37600,2);
    q15(1:9101,i)=Data(46500:55600,2);
    q2(1:9101,i)=Data(64500:73600,2);
    q25(1:9101,i)=Data(82500:91600,2);
    q3(1:9101,i)=Data(100500:109600,2);
end

%finding maximum absorbance values for
%the imported data range
for i=1:3
    Maxq05=max(q05(:,1:i));
    Maxq1=max(q1(:,1:i));
    Maxq15=max(q15(:,1:i));
    Maxq2=max(q2(:,1:i));
    Maxq25=max(q25(:,1:i));
    Maxq3=max(q3(:,1:i));
end

%finding minimum absorbance values for
%the imported data range
for i=1:3
    Minq05=min(q05(:,1:i));
    Minq1=min(q1(:,1:i));
    Minq15=min(q15(:,1:i));
    Minq2=min(q2(:,1:i));
    Minq25=min(q25(:,1:i));
    Minq3=min(q3(:,1:i));
end

end

%Normalizing concentration and taking
```

```

%the natural log of the normalized concentration
for i=1:3
    b05=q05(:,1:i)-Minq05(1,1:i);
    b1=q1(:,1:i)-Minq1(1,1:i);
    b15=q15(:,1:i)-Minq15(1,1:i);
    b2=q2(:,1:i)-Minq2(1,1:i);
    b25=q25(:,1:i)-Minq25(1,1:i);
    b3=q3(:,1:i)-Minq3(1,1:i);
    c05=b05./(Maxq05(1,1:i)-Minq05(1,1:i));
    c1=b1./(Maxq1(1,1:i)-Minq1(1,1:i));
    c15=b15./(Maxq15(1,1:i)-Minq15(1,1:i));
    c2=b2./(Maxq2(1,1:i)-Minq2(1,1:i));
    c25=b25./(Maxq25(1,1:i)-Minq25(1,1:i));
    c3=b3./(Maxq3(1,1:i)-Minq3(1,1:i));
    logc05=log10(c05(:,1:i));
    logc1=log10(c1(:,1:i));
    logc15=log10(c15(:,1:i));
    logc2=log10(c2(:,1:i));
    logc25=log10(c25(:,1:i));
    logc3=log10(c3(:,1:i));
end

%Defining time ranges for plotting
tt=Data(1600:10700,1);
tt1=Data(10800:19900,1);
tt2=Data(20000:29100,1);
tmin=min(tt);
tmin1=min(tt1);
tmin2=min(tt2);
tnorm=tt-tmin;
tnorm1=tt1-tmin1;
tnorm2=tt2-tmin2;
tnorm3=tnorm1(1:9101,1);

%figures 1 through 6 plot normalized concentration vs time
%for each flow rate
figure(1)
plot(tnorm,logc05(:,1))
xlabel('Normalized time,min')
ylabel('ln(C/Co)')
title('Configuration Comparison 0.5/min')

hold on
x2=logc05(:,2);
plot(tnorm,x2)
x3=logc05(:,3);
plot(tnorm,x3)
legend('Full','Pump2DAD','ValveSwitching')
hold off

figure(2)
plot(tnorm1,logc1(:,1))
xlabel('time,min')
ylabel('Normalized concentration')
title('Configuration Comparison 1ml/min')
hold on
x5=logc1(:,2);
plot(tnorm1,x5)

```

```

x6=logc1(:,3);
plot(tnorm1,x6)
legend('Full','Pump2DAD','ValveSwitching')
hold off

```

```

figure(3)
plot(tnorm1,logc15(:,1))
xlabel('time,min')
ylabel('Normalized concentration')
title('Configuration Comparison 1.5ml/min')
hold on
x8=logc15(:,2);
plot(tnorm1,x8)
x9=logc15(:,3);
plot(tnorm1,x9)
legend('Full','Pump2DAD','ValveSwitching')
hold off

```

```

figure(4)
plot(tnorm1,logc2(:,1))
xlabel('time,min')
ylabel('Normalized concentration')
title('Configuration Comparison 2ml/min')
hold on
x11=logc2(:,2);
x12=logc2(:,3);
plot(tnorm1,x11)
plot(tnorm1,x12)
legend('Full','Pump2DAD','ValveSwitching')
hold off

```

```

figure(5)
plot(tnorm1,logc25(:,1))
xlabel('time,min')
ylabel('Normalized concentration')
title('Configuration Comparison 2.5ml/min')
hold on
x13=logc25(:,2);
x14=logc25(:,3);
plot(tnorm1,x13)
plot(tnorm1,x14)
legend('Full','Pump2DAD','ValveSwitching')
hold off

```

```

figure(6)
plot(tnorm1,logc3(:,1))
xlabel('time,min')
ylabel('Normalized concentration')
title('Configuration Comparison 3ml/min')
hold on
x15=logc3(:,2);
x16=logc3(:,3);
plot(tnorm1,x15)
plot(tnorm1,x16)
legend('Full','Pump2DAD','ValveSwitching')
hold off

```

```

%Indexing to determine the linear short time region

```

```

%for plotting and solving for residence time
[~,index1]=min((tnorm-0.8).^2);
[~,index2]=min((tnorm-0.9).^2);
[~,index3]=min((tnorm1-2.7).^2);
[~,index4]=min((tnorm1-2.8).^2);
[~,index5]=min((tnorm2-2.7).^2);
[~,index6]=min((tnorm2-2.8).^2);
[~,index7]=min((tnorm-0.4).^2);
[~,index8]=min((tnorm-0.46).^2);
[~,index9]=min((tnorm-1.86).^2);
[~,index10]=min((tnorm-1.88).^2);
[~,index11]=min((tnorm-1.74).^2);
[~,index12]=min((tnorm-1.75).^2);
[~,index13]=min((tnorm-0.27).^2);
[~,index14]=min((tnorm-0.28).^2);
[~,index15]=min((tnorm-1.3).^2);
[~,index16]=min((tnorm-1.32).^2);
[~,index17]=min((tnorm-1.3).^2);
[~,index18]=min((tnorm-1.4).^2);
[~,index19]=min((tnorm-0.19).^2);
[~,index20]=min((tnorm-0.2).^2);
[~,index21]=min((tnorm-0.9).^2);
[~,index22]=min((tnorm-0.92).^2);
[~,index23]=min((tnorm-0.87).^2);
[~,index24]=min((tnorm-0.88).^2);
[~,index25]=min((tnorm-0.17).^2);
[~,index26]=min((tnorm-0.19).^2);
[~,index27]=min((tnorm-0.544).^2);
[~,index28]=min((tnorm-0.556).^2);
[~,index29]=min((tnorm-0.515).^2);
[~,index30]=min((tnorm-0.535).^2);
[~,index31]=min((tnorm-0.13).^2);
[~,index32]=min((tnorm-0.14).^2);
[~,index33]=min((tnorm-0.14).^2);
[~,index34]=min((tnorm-0.168).^2);
[~,index35]=min((tnorm-0.14).^2);
[~,index36]=min((tnorm-0.16).^2);

%Solving for residence time using the previous indexes of the
%short time region by using polyfit for a first order polynomial
%to find the slope which is related to residence time

%Flowrate of 0.5ml/min (Order: 'Full', 'Pump2DAD', 'ValveSwitching')
taui1=polyfit(tnorm(index1:index2),logc05(index1:index2,1),1);
tau1=(-1/taui1(1,1))*60;
taui2=polyfit(tnorm(index3:index4),x2(index3:index4),1);
tau2=(-1/taui2(1,1))*60;
taui3=polyfit(tnorm(index5:index6),x3(index5:index6),1);
tau3=(-1/taui3(1,1))*60;

%Flowrate of 1ml/min (Order: 'Full','Pump2DAD','ValveSwitching')
taui4=polyfit(tnorm(index7:index8),logc1(index7:index8,1),1);
tau4=(-1/taui4(1,1))*60;
taui5=polyfit(tnorm1(index9:index10),x5(index9:index10),1);
tau5=(-1/taui5(1,1))*60;
taui6=polyfit(tnorm1(index11:index12),x6(index11:index12),1);
tau6=(-1/taui6(1,1))*60;

```

```

%Flowrate of 1.5ml/min (Order: 'Full','Pump2DAD','ValveSwitching')
tau7=polyfit(tnorm1(index13:index14),logc15(index13:index14,1),1);
tau7=(-1/tau7(1,1))*60;
tau8=polyfit(tnorm1(index15:index16),x8(index15:index16),1);
tau8=(-1/tau8(1,1))*60;
tau9=polyfit(tnorm1(index17:index18),x9(index17:index18),1);
tau9=(-1/tau9(1,1))*60;

%Flowrate of 2ml/min ('Full','Pump2DAD','ValveSwitching')
tau10=polyfit(tnorm(index19:index20),logc2(index19:index20,1),1);
tau10=(-1/tau10(1,1))*60;
tau11=polyfit(tnorm(index21:index22),x11(index21:index22),1);
tau11=(-1/tau11(1,1))*60;
tau12=polyfit(tnorm1(index23:index24),x12(index23:index24),1);
tau12=(-1/tau12(1,1))*60;

%Flowrate of 2.5ml/min ('Full','Pump2DAD','ValveSwitching')
tau13=polyfit(tnorm(index25:index26),logc25(index25:index26,1),1);
tau13=(-1/tau13(1,1))*60;
tau14=polyfit(tnorm(index27:index28),x13(index27:index28),1);
tau14=(-1/tau14(1,1))*60;
tau15=polyfit(tnorm1(index29:index30),x14(index29:index30),1);
tau15=(-1/tau15(1,1))*60;

%Flowrate of 3ml/min ('Full','Pump2DAD','ValveSwitching')
tau16=polyfit(tnorm(index31:index32),logc3(index31:index32,1),1);
tau16=(-1/tau16(1,1))*60;
tau17=polyfit(tnorm(index33:index34),x15(index33:index34),1);
tau17=(-1/tau17(1,1))*60;
tau18=polyfit(tnorm1(index35:index36),x16(index35:index36),1);
tau18=(-1/tau18(1,1))*60;

%Defining flow rates, ml/min
f=0.5;
f1=1;
f2=1.5;
f3=2;
f4=2.5;
f5=3;

%changing flow rates to inverse flow rate in units
%of sec/ml
fa=(1/f)*60;
f1a=(1/f1)*60;
f2a=(1/f2)*60;
f3a=(1/f3)*60;
f4a=(1/f4)*60;
f5a=(1/f5)*60;

%Organizing Residence time of each flow rate into matrices
%for each configuration

%Order: Pump2dad, Novalve, Noinject,Full
y=[tau1 tau4 tau7 tau10 tau13 tau16 0];
y1=[tau2 tau5 tau8 tau11 tau14 tau17 0];
y2=[tau3 tau6 tau9 tau12 tau15 tau18 0];

```

```

%Creating a matrix of inverse flow rates
z=[fa f1a f2a f3a f4a f5a 0];

%Plotting only the linear short time region based on
%indexed values to check for accuracy in figures
%7 through 12
figure(7)
plot(tnorm(index1:index2),logc05(index1:index2,1),'-o')
xlabel('time,min')
ylabel('log10(C/Co)')
title('Config Compare 0.5ml/min')
hold on
plot(tnorm(index3:index4),x2(index3:index4),'-^')
plot(tnorm(index5:index6),x3(index5:index6),'-x')
legend('Full', 'Pump2DAD', 'ValveSwitch')
hold off

figure(8)
plot(tnorm1(index7:index8),logc1(index7:index8),'-o')
xlabel('time,min')
ylabel('log10(C/Co)')
title('Config Compare 1ml/min')

hold on

plot(tnorm1(index9:index10),x5(index9:index10),'-^')
plot(tnorm1(index11:index12),x6(index11:index12),'-x')
legend('Full', 'Pump2DAD', 'ValveSwitch')
hold off

figure(9)
plot(tnorm1(index13:index14),logc15(index13:index14),'-o')
xlabel('time,min')
ylabel('log10(C/Co)')
title('Config Compare 1.5ml/min')

hold on
plot(tnorm2(index15:index16),x8(index15:index16),'-^')
plot(tnorm2(index17:index18),x9(index17:index18),'-x')
legend('Full', 'Pump2DAD', 'ValveSwitch')
hold off

figure(10)
plot(tnorm1(index19:index20),logc2(index19:index20,1),'-o')
xlabel('time,min')
ylabel('log10(C/Co)')
title('Config Compare 2ml/min')
hold on
plot(tnorm1(index21:index22),x11(index21:index22),'-^')
plot(tnorm1(index23:index24),x12(index23:index24),'-x')
legend('Full', 'Pump2DAD', 'ValveSwitch')
hold off

figure(11)
plot(tnorm1(index25:index26),logc25(index25:index26,1),'-o')
xlabel('time,min')

```

```

ylabel('log10(C/Co)')
title('Config Compare 2.5ml/min')
hold on
plot(tnorm1(index27:index28),x13(index27:index28),'-^')
plot(tnorm1(index29:index30),x14(index29:index30),'-x')
legend('Full', 'Pump2DAD','ValveSwitch')
hold off

figure(12)
plot(tnorm2(index31:index32),logc3(index31:index32,1),'-O')
xlabel('time,min')
ylabel('log10(C/Co)')
title('Config Compare 3ml/min')
hold on
plot(tnorm2(index33:index34),x15(index33:index34),'-^')
plot(tnorm2(index35:index36),x16(index35:index36),'-x')
legend('Full', 'Pump2DAD','ValveSwitch')
hold off

%plot of residence time vs inverse flow rate
%and using polyfit for a first order polynomial
%to find slope aka dead volume
figure(13)
plot(z,y,'-O') %Full
xlabel('inverse flow rate, (seconds/mL)')
ylabel('Residence time, tau (seconds)')
title('Configuration Comparison 6 flows')
hold on
plot(z,y1,'-^') %Pump2dad
plot(z,y2,'-x') %valveswitch
legend('Full', 'Pump2DAD','ValveSwitch')
hold off

%v symbolizes dead volume which is solved by dividing inverse flow rate
%by residence times using the least squares method
%Lower 3 flows
v=z(:)\y(:);
v1=z(:)\y1(:);
v2=z(:)\y2(:);

%putting dead volumes for each configuration in a vector
%for graphing purposes
vall=[v(1,1) v1(1,1) v2(1,1)];
vall1=[v1(1,1) v2(1,1)];

%Bar graphs for dead volume at different configurations
figure(15)
name={'Full';'Pump2DAD';'ValveSwitch'};
bar(vall)
ylabel('Dead Volume, ml')
set(gca,'xticklabel',name)
title('Dead Volume Graph')

%Checking accuracy of polyfit for index to ensure
%the region used for residence time is accurately modeled using

```

```
%polyfit
figure(16)
plot(tnorm1,x14)
xlabel('time,min')
ylabel('ln(C/Co)')
title('2.5 ml/min ValveSwitch')
axis([0 6 -6 0.1])
taufit=taui15(1,1)*tnorm1+taui15(1,2);
hold on
plot(tnorm1,taufit)
legend('Actual','Polyfit')
hold off
```

## Script 2: Numerical\_PDE\_MAIN.m

This script evaluates the overall mass balance based on initial guesses for parameters like diffusion and flow rate. The diffusion coefficient guess, initial concentration vector, time vector, and flow rates are defined in this script. The concentration of paracetamol as a function of radius and concentration in the mobile liquid phase from desorption are both plotted and parameters are changed until the HPLC data is accurately represented by the model. The parameters defined in `bvpscripts.m` are referenced here.

```
function res = Numerical_PDE_MAIN(param, t, thetaexp, plotson)
% Purpose of this code is to evaluate unsteady dispersion model for
% a step input PBR
%Inputs
%param = [L log10D]
%t = time vector
%thetaexp = experimental data of length t
%plotson = 1 for displaying all plots, 0 for displaying only fit

%Outputs
%res = Error to be minimized for fit

%% Inputs
Dab = 10^param(2); %m^2/s change time scale and/or time steps when
changing Dab
L = param(1); %Fitting parameter defined by Brandani & Ruthven
(1995)
ntau = length(t); % Increments in tau
tauf = t(end); % Final value for tau % s
nx = 150; % Increments in x %

% Initial Condition
theta0 = ones(nx+1,1); % % Initial concentration profile

%% Define Variables

% Discretize Variables
tau = linspace(0,tauf,ntau);
x = linspace(1e-10,7e-6,nx+1); % 14 um particle
theta = ones(nx+1,ntau);
theta(:,1) = theta0;

%% Solve PDE

y0 = ones(size(theta0))*0.001;

for i = 2:ntau %Solving PDE from initial t to final t,
stepping through each sequential time step
    dtau = tau(i)-tau(i-1);
    if mod(i,10) == 0
        disp(['Status: ', num2str(i-1), ' of ', num2str(ntau-1)])
    end
    y0 = theta(:,i-1);
    y = bvpscripts(Dab,y0,x,dtau,L);
    theta(1:end,i) = y;
end
```

```

    res = (log(theta(end-1,:)) - log(thetaexp')).^2;           %Error between
experimental data and model being minimized by ZLC_Fits

%% Plots

figure(1)
hold on
semilogy(t,thetaexp,'b-',t,theta(end-1,:),'-')
set(gca,'YScale','log')
title(['X = ' num2str(param)])
drawnow
hold off

if plotson == 1
    figure(2);
    plot(x,theta(1:end,:))
    xlabel('r, [m]')
    ylabel('\theta = C/C_0, [ - ]')

    figure(3);
    surf(tau,x,theta)
    xlabel('time, [s]')
    ylabel('r, [m]')
    zlabel('\theta = C/C_0, [ - ]')

    figure(4);
    plot(tau,theta(1,:),tau,theta(end,:))
    legend('Center','Surface')
    xlabel('time, [s]')
    ylabel('\theta = C/C_0, [ - ]')
end
end

```

### Script 3: bvpscripts.m

This script is used to define and solve the boundary conditions for solving the mass balance equation for the ZLC. The overall mass balance equation is defined as well. This is solved simultaneously with the numerical pde script to model the HPLC data.

```
function res = Numerical_PDE_MAIN(param, t, thetaexp, plotson)
% Purpose of this code is to evaluate unsteady dispersion model for
% a step input PBR
%Inputs
    %param = [L log10D]
    %t = time vector
    %thetaexp = experimental data of length t
    %plotson = 1 for displaying all plots, 0 for displaying only fit

%Outputs
    %res = Error to be minimized for fit

%% Inputs
    Dab = 10^param(2); %m^2/s    change time scale and/or time steps when
changing Dab
    L = param(1);    %Fitting parameter defined by Brandani & Ruthven
(1995)
    ntau = length(t);    % Increments in tau
    tauf = t(end);    % Final value for tau % s
    nx = 150;    % Increments in x %

% Initial Condition
theta0 = ones(nx+1,1); % % Initial concentration profile

%% Define Variables

% Discretize Variables
tau = linspace(0,tauf,ntau);
x = linspace(1e-10,7e-6,nx+1); % 14 um particle
theta = ones(nx+1,ntau);
theta(:,1) = theta0;

%% Solve PDE

y0 = ones(size(theta0))*0.001;

for i = 2:ntau    %Solving PDE from initial t to final t,
stepping through each sequential time step
    dtau = tau(i)-tau(i-1);
    if mod(i,10) == 0
        disp(['Status: ', num2str(i-1), ' of ', num2str(ntau-1)])
    end
    y0 = theta(:,i-1);
    y = bvpscripts(Dab,y0,x,dtau,L);
    theta(1:end,i) = y;
end
```

```

    res = (log(theta(end-1,:)) - log(thetaexp')).^2;           %Error between
experimental data and model being minimized by ZLC_Fits

%% Plots

figure(1)
hold on
semilogy(t,thetaexp,'b-',t,theta(end-1,:),'-')
set(gca,'YScale','log')
title(['X = ' num2str(param)])
drawnow
hold off

if plotson == 1
    figure(2);
    plot(x,theta(1:end,:))
    xlabel('r, [m]')
    ylabel('\theta = C/C_0, [ - ]')

    figure(3);
    surf(tau,x,theta)
    xlabel('time, [s]')
    ylabel('r, [m]')
    zlabel('\theta = C/C_0, [ - ]')

    figure(4);
    plot(tau,theta(1,:),tau,theta(end,:))
    legend('Center','Surface')
    xlabel('time, [s]')
    ylabel('\theta = C/C_0, [ - ]')
end
end

```

## Script 4: ZLC\_Fits.m

```
%% ZLC Analysis

%The purpose of this code is to iterate through a number of guesses to
%attempt to converge to a PDE model that matches the given experimental
%data

close all
clear
clc

%% Inputs
%Normalized desorption profile
thetadata = downsample(dlmread('NaTrial2.csv'), 20); %Downsampling to
every 20th row
t = thetadata(1:301,1); %time column
thetaexp = thetadata(1:301,2); %normalized concentration column

%% Guesses
log10D = -12.15; %log10(diffusion constant)
L0 = 200; % dimesnionless, 1 - 10000 (bigger = better)

%% Parse Input Data
x0 = [L0 log10D];

%% Fit ZLC
[x, error] = lsqnonlin(@Numerical_PDE_MAIN,x0,[175 -13],[10000 -12],[ ], t,
thetaexp, 0); %Iterative solution based on non linear least squares fit
```

## Appendix C: SDS Sheets

### Sodium Nitrate

[https://beta-static.fishersci.com/content/dam/fishersci/en\\_US/documents/programs/education/regulatory-documents/sds/chemicals/chemicals-s/S25558B.pdf](https://beta-static.fishersci.com/content/dam/fishersci/en_US/documents/programs/education/regulatory-documents/sds/chemicals/chemicals-s/S25558B.pdf)

### Terephthalic Acid

<https://www.fishersci.com/shop/msdsproxy?productName=AC321440010&productDescription=TEREPHTHALIC-D4+ACID%2C+1G&catNo=AC32144-0010&vendorId=VN00032119&storeId=10652>

### Zeolite Y and Na-Y

<https://www.fishersci.com/store/msds?partNumber=AA4586214&productDescription=ZEOLITE+Y%2C+SODIUM+25G&vendorId=VN00024248&countryCode=US&language=en>

### Zinc Nitrate Hexahydrate

<https://www.fishersci.com/shop/msdsproxy?productName=Z45500&productDescription=ZINC+NITRATE+CRYSTAL+CERT+500G&catNo=Z45-500&vendorId=VN00033897&storeId=10652>

### Diethylformamide

<https://www.fishersci.com/shop/msdsproxy?productName=AC181370250&productDescription=N%2CN-DIETHYLFORMAMIDE%2C+99+25ML&catNo=AC181370250&vendorId=VN00032119&storeId=null>